食餌中の亜硝酸塩および硝酸塩の不足は代謝症候群、内皮機能不全、および心血管死を惹起する

Long-Term Dietary Nitrite and Nitrate Deficiency Causes Metabolic Syndrome, Endothelial Dysfunction, and Cardiovascular Death in Mice

Mika Kina-Tanada[1,2,*], Mayuko Sakanashi[1,*], Akihide Tanimoto[3], Tadashi Kaname[4], Toshihiro Matsuzaki[1], Katsuhiko Noguchi[1], Taro Uchida[1], Junko Nakasone[1], Chisayo Kozuka[5], Masayoshi Ishida[1,6], Haruaki Kubota[1], Yuji Taira[1], Yuichi Totsuka[1], Shin-ichiro Kina[2], Hajime Sunakawa[2], Junichi Omura[7], Kimio Satoh[7], Hiroaki Shimokawa[7], Nobuyuki Yanagihara[8], Shiro Maeda[4], Yusuke Ohya[9], Masayuki Matsushita[10], Hiroaki Masuzaki[5], Akira Arasaki[2], and Masato Tsutsui[1]

Departments of [1]Pharmacology, [2]Oral and Maxillofacial Functional Rehabilitation, [4]Advanced Genomic and Laboratory Medicine, and [10]Physiology, [5]Second and [9]Third Departments of Internal Medicine, and [6]Regenerative Medicine Research Center, Graduate School of Medicine, University of the Ryukyus, Okinawa, Japan; [3]Department of Pathology, Kagoshima University Graduate School of Medical and Dental Sciences, Kagoshima, Japan; [7]Department of Cardiovascular Medicine, Tohoku University Graduate School of Medicine, Sendai, Japan; and [8]Department of Pharmacology, School of Medicine, University of Occupational and Environmental Health, Kitakyushu, Japan

*These authors contributed equally to this work.

Short running title:
Dietary NOx deficiency causes MetS and CVD

Word count:
Abstract: 260; Main text: 3991 with 4 tables, 8 figures, and 4 ESM figures

Address for correspondence:
Masato Tsutsui, MD, PhD, Professor and Chairman, Department of Pharmacology, Graduate School of Medicine, University of the Ryukyus, 207 Uehara, Nishihara, Okinawa 903-0215, Japan. Phone: +81-98-895-1133; Fax: +81-98-895-1411; E-mail: tsutsui@med.u-ryukyu.ac.jp

Abstract

Aims/hypothesis Nitric oxide (NO) is synthesized not only from L-arginine by NO synthases (NOSs), but also from its inert metabolites, nitrite and nitrate. Green leafy vegetables are abundant in nitrate, however whether or not a deficiency in dietary nitrite/nitrate spontaneously causes disease remains to be clarified. In this study, we tested our hypothesis that long-term dietary nitrite/nitrate deficiency induces metabolic syndrome (MetS) in mice.

Methods To this end, we prepared a low nitrite/nitrate diet (LND) consisting of an amino acid-based low nitrite/nitrate chow in which the contents of L-arginine, fat, carbohydrates, protein, and energy were identical with a regular chow, and potable ultrapure water. Nitrite and nitrate were undetectable in both the chow and the water.

Results Three months of the LND did not affect food or water intake in wild-type C57BL/6J mice as compared with a regular diet (RD). However, in comparison with the RD, 3 months of the LND significantly elicited visceral adiposity, dyslipidaemia, and glucose intolerance; 18 months of the LND significantly provoked increased body weight, hypertension, insulin resistance, and impaired endothelium-dependent relaxations to acetylcholine; and 22 months of the LND significantly led to death due to cardiovascular disease, including acute myocardial infarction. These abnormalities were reversed by simultaneous treatment with sodium nitrate, and were significantly associated with endothelial NOS down-regulation, adiponectin insufficiency, and gut microbiota dysbiosis.

Conclusions/interpretation These results provide the first evidence that long-term dietary nitrite/nitrate deficiency gives rise to MetS, endothelial dysfunction, and cardiovascular death in mice, indicating a novel pathogenetic role of the exogenous NO production system in MetS and its vascular complications.

Key words: acute myocardial infarction, cardiovascular death, diet, endothelial dysfunction, metabolic syndrome, mice, nitrite, nitrate, nitric oxide

Abbreviations:

AMPK	adenosine monophosphate-activated protein kinase
DEA-NONOate	diethylamine-NONOate
eNOS	endothelial nitric oxide synthase
EWAT	epididymal white adipose tissue
iNOS	inducible nitric oxide synthase
LND	a low nitrite/nitrate diet
MetS	metabolic syndrome
nNOS	neuronal nitric oxide synthase
NO	nitric oxide
NOS	NO synthase
p-AMPK	phosphorylated AMPK
PPAR-γ	peroxisome proliferator-activated receptor-gamma
RD	a regular diet
WAT	white adipose tissue
WT	wild-type

Introduction

Metabolic syndrome (MetS) is defined as a constellation of interrelated cardiovascular risk factors of metabolic origin, including visceral obesity, dyslipidaemia, hypertension, glucose intolerance, and insulin resistance [1]. MetS is highly prevalent in industrial countries worldwide, and it has been reported that, in accordance with the most recent harmonized definition of MetS, 23% of the adult population (≥20 years) in America suffered from MetS in 2009-2010 [2, 3]. Greater global industrialization is associated with rising rates of obesity, which are expected to dramatically increase the prevalence of MetS in the world, especially as the population ages [1]. MetS is associated with increased risks of myocardial infarction, stroke, cardiovascular disease mortality, and all-cause mortality [4]. MetS also confers higher risks of peripheral vascular disease, type 2 diabetes, renal disease, hepatic disease, and cancer [5-9]. Several factors, including excessive food energy intake, lack of physical activity, genetic susceptibility, and aging, have been thought to be involved in the pathogenesis of MetS. However, the precise mechanisms in the development of MetS still remain to be fully elucidated [1].

Nitric oxide (NO) exerts multiple biological actions, and is one of the most crucial signalling molecules in mammalian physiology and pathology [10-15]. NO is endogenously synthesized from a precursor L-arginine by a family of NO synthases (neuronal [nNOS], inducible [iNOS], and endothelial NOS [eNOS]) with stoichiometric production of L-citrulline. NO has a very short half-life of several seconds, and is rapidly oxidized to nitrite (NO_2^-) and subsequently to nitrate (NO_3^-). Although nitrite and nitrate were regarded as mere inert NO metabolites in the past, recent studies have revealed that nitrate is reduced to nitrite and then to NO, serving as NO donors [16-18]. Green leafy vegetables, such as spinach, lettuce, and beetroot, are abundant in nitrate, and vegetables are the dominant source of dietary nitrate in humans, contributing to

60-80% of dietary nitrate intake [19, 20]. Potable tap water also contains nitrate and a small quantity of nitrite, and 15-20% of dietary nitrate intake is derived from tap water [19, 20]. It has been reported that cardiac and hepatic ischaemia-reperfusion injury in mice [21-23], cardiac allograft rejection in rats [23], and platelet aggregation in mice [24] are exacerbated by a low nitrite/nitrate diet (LND) (a commercially available low nitrite/nitrate chow plus potable ultrapure water, or the low nitrite/nitrate chow alone) as compared with a regular diet (RD). These results suggest that dietary nitrite/nitrate deficiency modulates disease conditions. Whether or not this deficiency spontaneously causes disease, however, remains to be clarified. In this study, we tested our hypothesis that long-term dietary nitrite/nitrate deficiency gives rise to MetS in mice.

Methods

Mice

This study was approved by the Animal Care and Use Committee, the University of the Ryukyus, Japan, and was carried out according to the Institutional Policy on the Care and Use of the Laboratory Animals. The experiments were performed in 6-week-old male wild-type (WT) C57BL/6J mice (Kyudo, Co., Inc., Tosu, Japan). All the mice were maintained in temperature- and humidity-controlled rooms illuminated from 8:00 a.m. to 8:00 p.m. Food and water intake was measured by placing the animals in metabolic cages for 24 hours (see electronic supplementary material [ESM] Methods for further details).

Diet

We prepared a purified amino acid-based low nitrite and nitrate chow in which the contents of L-arginine, fat, carbohydrates, protein, and energy were identical to a regular chow (Purina 5001, LabDiet, St. Louis, MO) and potable ultrapure milli Q water in which nitrite and nitrate levels were undetectable (Merck Millipore, Darmstadt, Germany) (Tables 1 and 2). Either the low nitrite/nitrate chow plus ultrapure water (LND) or the regular chow plus tap water (RD) was fed *ad libitum* to the mice from 6 weeks of age for 1.5-22 months. See ESM Methods.

Nitrite and Nitrate Levels

The nitrite and nitrate contents in the chows were analysed by the diazotization method and the cadmium reduction-diazotization method, respectively (Japan Food Research Laboratories, Tokyo, Japan). The nitrite and nitrate levels in the plasma and drinking water were assessed by the HPLC-Griess system (ENO-20, Eicom, Kyoto, Japan). See ESM Methods.

Blood Pressure

Systolic blood pressure was measured by the tail-cuff method under conscious conditions in a blind manner (Model MK-2000, Muromachi Kikai, Co., Inc., Tokyo, Japan). See ESM Methods.

Glucose Tolerance Test

One g of glucose per kg body weight was intraperitoneally injected into the mice under general anaesthesia with sodium pentobarbital (50 mg/kg, IP, Sigma-Aldrich, St. Louis, MO, USA) after 18 hours of fasting. Whole blood samples were collected from the tail, and the blood glucose levels were evaluated by a portable blood glucose analyser (Glucocard MyDia, Arkray, Inc., Kyoto, Japan). See ESM Methods.

Insulin Tolerance Test and Plasma Insulin

The mice received 0.3 unit/kg body weight insulin (Eli Lilly, Indianapolis, IN) injected into the intraperitoneal cavity under general anaesthesia with sodium pentobarbital (50 mg/kg, IP). The fasting plasma insulin levels were assessed by a commercially available ELISA kit (AKRIN-031, Shibayagi, Gunma, Japan). See ESM Methods.

Visceral Fat Weight

After euthanasia, epididymal white adipose tissues (EWAT) were removed and weighed. See ESM Methods.

Adipocyte Hypertrophy and Inflammation

Epididymal and peri-renal white adipose tissues (WAT) were stained with a haematoxylin-eosin solution. The circumferential length of each adipocyte was measured by a light microscope equipped with a CCD camera and morphometric analysis software (DS-Ri1CCD camera and NIS-Elements D 3.2 software, Nikon,

Tokyo, Japan). For evaluation of inflammation in the adipose tissues, aggregates of inflammatory cells (inflammatory foci consisting of more than 10 inflammatory cells) were counted in the maximal cut surface of the epididymal and the peri-renal WAT sections on a light microscope at 40x magnification. See ESM Methods.

Plasma Lipid Profile

Plasma lipid profile was assessed by a Dri-Chem autoanalyser (FDC4000, Fuji Film Co., Ltd., Tokyo, Japan). Plasma low-density lipoprotein (LDL) cholesterol levels were determined by the high-performance liquid chromatography (Skylight Biotech Inc., Akita, Japan) [25]. See ESM Methods.

Western Blot Analysis

To detect nNOS, iNOS, and eNOS, phosphorylated eNOS at serine 1177 and at threonine 495 (BD Transduction Laboratories, Franklin Lakes, NJ), adiponectin, peroxisome proliferator-activated receptor-γ (PPAR-γ), adenosine monophosphate-activated protein kinase (AMPK), sirtuin1 (Cell Signaling Technology, Danvers, MA), phosphorylated AMPK (p-AMPK, Santa Cruz Biotechnology Inc., Dallas, TX) and glyceraldehyde-3-phosphate dehydrogenase (GAPDH) (Sigma-Aldrich), Western blot analysis was performed as we previously reported [26]. See ESM Methods.

Serum Cytokine and Chemokine Levels

Serum cytokine/chemokine levels were measured with a Bio-Plex system (23-Plex, M60-009RDPD, Bio-Rad, CA, USA) [27].

16S Ribosomal RNA Gene Sequencing

The faecal DNA samples were subjected to a next generation sequencer, as reported

previously [28]. The number of each bacterial strain contained in the faecal contents was estimated as the genome equivalent by quantitative real-time PCR of 16S ribosomal RNA genes, followed by pyrosequencing of the 16S amplicons [28]. See ESM Methods.

Organ Chamber Experiment

The thoracic aortic rings were mounted in microtissue organ bath chambers (MTBO-1, Labo Support, Osaka, Japan) filled with Krebs-Henseleit solution, and the isometric contractile force of the rings was measured. See ESM Methods.

Micro-Computed Tomography (CT) Imaging

Mice were anesthetized with 2% isoflurane (Wako Pure Chemical), and CT images were acquired by three-dimensional micro-CT (R_mCT2; Rigaku Corporation, Tokyo, Japan). See ESM Methods.

Statistical Analyses

Most of our results are expressed as mean ± SEM, and the statistical analyses were performed by a Student's *t*-test, or ANOVA followed by Bonferroni's *post hoc* test. The results of sequencing reads of gut bacteria are expressed as the median and interquartile range, and the statistical analysis was carried out by a Wilcoxon rank-sum test [29]. Kaplan-Meier survival curves were compared by the log-rank test. A value of $p<0.05$ was considered to be statistically significant. See ESM Methods.

Results

3-Month LND Markedly Reduced Plasma Nitrite/Nitrate Levels

We prepared the LND consisting of an amino acid-based low nitrite/nitrate chow in which the contents of L-arginine, fat, carbohydrates, protein, and energy were identical with a regular chow, and potable ultrapure water (Tables 1 and 2). Nitrite and nitrate were undetectable in both the chow and the water (Tables 1 and 2). WT C57BL/6J mice were fed either the LND (the low nitrite/nitrate chow plus the drinking ultrapure water) or the RD (the regular chow plus tap water) on a long-term basis.

The 3-month LND markedly reduced the plasma nitrite/nitrate levels as compared with the RD (Fig. 1a). To examine this mechanism, we evaluated the NOS expression levels in isolated aorta and visceral fat. The eNOS protein levels in the aorta were comparable in the two diets (Fig. 1b), whereas, intriguingly, those levels in the EWAT were markedly lower in the LND than in the RD (Fig. 1c), accounting for the markedly reduced plasma nitrite/nitrate levels induced by the LND. There was no expression of nNOS or iNOS in the EWAT in either diet (ESM Fig. 1a).

3-Month LND Resulted in MetS-Like Conditions

There were no significant differences in food intake (Fig. 1d), water intake (ESM Fig. 1b), or body weight (ESM Fig. 1c) between the 3-month LND and RD. However, the 3-month LND significantly increased EWAT weight (Fig. 1e), epididymal white adipocyte size (Fig. 1f), and plasma levels of total cholesterol (Fig. 2a), LDL cholesterol (Fig. 2b), and small dense LDL cholesterol (ESM Fig. 1d), and tended to elevate plasma triacylglycerol levels as compared with the RD (Table 3). Furthermore, the 3-month LND significantly augmented blood glucose levels after intraperitoneal glucose injection and aggravated blood glucose-lowering responses to intraperitoneal insulin injection (Fig. 2d,g and ESM Fig. 1f). The arterial blood pressure levels were similar

in both diets (ESM Fig. 2a).

We next studied the time course of the metabolic effects at 1.5, 3, and 4.5 months after the start of the LND. The effects on the EWAT weight (Fig. 1e), the plasma total cholesterol levels (Fig. 2a), the blood glucose levels after glucose injection (Fig. 2c-e), and the blood glucose-lowering responses to insulin (Fig. 2f-h and ESM Fig. 1e-g) were time-dependent, and appeared to reach a plateau at 3 months. There were no significant differences in the fasting plasma insulin levels between the mice fed the LND and the RD at any of the time points (ESM Fig. 2b).

The adiponectin levels in the EWAT were markedly lower in the 3-month LND as compared with the RD (Fig. 3a). The levels in the EWAT of PPAR-γ, total AMPK, and p-AMPK, but not sirtuin1, were also markedly reduced in the 1-week LND in comparison to the RD (Fig. 3b-e).

Simultaneous oral treatment with 2 mmol/l sodium nitrate for 3 months significantly reversed the reduced plasma nitrite/nitrate levels induced by the LND (Fig. 4a). It also tended to improve the LND-induced gain in the EWAT weight (Fig. 4b), and significantly ameliorated the epididymal white adipocyte hypertrophy, hyper-small dense LDL cholesterolemia, impaired glucose tolerance, the reduced blood glucose-lowering responses to insulin, eNOS down-regulation, and adiponectin insufficiency induced by the LND (Fig. 4c-h and ESM Fig. 2c).

Dysbiosis of Gut Microbiota Was Noted in the LND-Fed Mice

While there was no significant difference between the two diets in the total sequencing reads (ESM Fig. 3a), the operational taxonomic units, which represent the kind of gut bacteria, were significantly fewer in the LND than in the RD, suggesting less diversity of gut microbiota (Fig. 5a). Significantly different gut bacteria in each rank are shown in Fig. 5b,c and ESM Fig. 3b-j. In the phylum rank, there were more Actinobacteria in the LND than in the RD (ESM Fig. 3b). In the class rank, there were more

Actinobacteria and fewer Betaproteobacteria in the LND (ESM Fig. 3c,d). In the order rank, Bifidobacteriales was more numerous in the LND, and Burkholderiales and Bacillales were less (ESM Fig. 3e,f). In the family (ESM Fig. 3g,h), the genus (Fig. 5b,c), and the species ranks (ESM Fig. 3i,j), more than 3 gut bacteria were more prevalent, and more than 2 gut bacteria were less prevalent in the LND. On the other hand, a certain amount of *Bacteroides fragilis* was present in the RD, but absent in the LND (312 [118-446] in RD vs. 0 in LND, median and interquartile range, n=5). There were no significant differences between the two diets in Firmicutes, Bacteroidetes, or the Firmicutes/Bacteroidetes ratio, which might change in disease states of MetS [30-33], or *Akkermansia muciniphila*, which might improve MetS [34, 35] (data not shown). *Bacteroides uniformis* CECT 7771, which might improve MetS [36], was not detected in either diet.

18-Month LND Resulted in More Severe MetS and Endothelial Dysfunction

Although the metabolic effects of the LND appeared to reach a plateau at 3 months, we explored the effects of an extremely long period of LND (18 months) for confirmation. There were no significant differences in food or water intake between the 18-month LND and RD (ESM Fig. 4a,b), but, notably, 18 months of the LND resulted in more severe MetS, eliciting a significant gain in body weight, which was not seen until 4.5 months after the start of the LND (Fig. 6a). Micro-CT imaging indicated that body fat was markedly increased, by 3.2 times, in the 18-month LND-fed mice (Fig. 6b,c), and this was specifically due to an increase in visceral fat (Fig. 6d), not in subcutaneous fat (ESM Fig. 4c). The 18-month LND elevated plasma small dense LDL levels and blood glucose levels following glucose injection, and significantly blunted blood glucose-lowering responses to insulin (Fig. 6e-g and ESM Fig. 4d). In addition, it significantly increased levels of fasting blood glucose, fasting plasma insulin, and arterial blood pressure (Fig. 7a-c), which findings were not observed until 4.5 months

after the start of the LND. The eNOS protein levels in the EWAT were also significantly decreased in the 18-month LND (ESM Fig. 4e).

Since the 18-month LND induced severe MetS, we next examined vascular reactivity. In isolated aortas, contractions to phenylephrine, an adrenergic α1 receptor agonist, and endothelium-independent relaxations to diethylamine (DEA)-NONOate, a NO donor, were comparable between the two diets (ESM Fig. 4f,g), whereas endothelium-dependent relaxations to acetylcholine, a physiological eNOS activator, were significantly impaired in the LND (Fig. 7d). The eNOS protein levels were significantly diminished in the aortas (Fig. 7e), and there was a tendency of lower phosphorylation levels of eNOS at serine 1177, which is an index of eNOS activation, without affecting the phosphorylation levels of eNOS at threonine 495, which is an index of eNOS inactivation, in the LND (ESM Fig. 4h,i).

Simultaneous treatment with sodium nitrate for 18 months inhibited these metabolic abnormalities, the endothelial dysfunction, and the aortic and EWAT eNOS down-regulation induced by the LND (Figs. 6 and 7a-e and ESM Fig. 4c-e).

There were no significant increases in the serum levels of 22 inflammatory markers measured by the Bio-Plex system between the 1.5-month LND and RD (Table 4). There were also no significant differences in the number of inflammatory foci in the EWAT and peri-renal WAT between the 3-month LND and RD (data not shown). However, the 18-month LND tended to increase the number of inflammatory foci in the EWAT and significantly augmented that in the peri-renal WAT compared with the RD (Fig. 7f,g).

22-Month LND Led to Cardiovascular Death

We experienced sudden death in some of the LND-fed mice. During the 22 months of follow-up, none (0/24) of the RD-fed mice died, whereas 31.8% (7/22) of the LND-fed mice passed away. The survival rate was significantly worse in the LND-fed than in

the RD-fed mice, and co-treatment with sodium nitrate improved the reduced survival (Fig. 8a). We performed a postmortem histopathological analysis in order to identify the cause of death in the 7 dead LND-fed mice. We could not examine the cause of death in 1 mouse because of strong postmortem putrefaction. We judged that 1 mouse died of acute myocardial infarction of the anterior wall (Fig. 8b), and that 1 mouse died of malignant lymphoma in the lung, liver (Fig. 8g), kidney, and spleen. In all the other 4 mice we noted coronary perivascular fibrosis, pulmonary congestion, and acute renal tubular necrosis (Fig. 8d-f), which findings are observed in cardiac sudden death. Myocardial fibrosis, which might have resulted from myocardial infarction, was seen in 1 mouse (Fig. 8c), malignant lymphoma in the liver and spleen was observed in 1 mouse, and no other pathological findings that could explain the cause of death were seen in any of the mice.

Discussion

In previous studies, the effects of a LND on cardiac and liver ischaemia-reperfusion injury [21-23], cardiac allograft rejection [23], and platelet aggregation [24] were studied by using a commercially available low nitrite/nitrate chow, but the contents of L-arginine, fat, carbohydrates, protein, and energy were considerably different between the commercially available low nitrite/nitrate chow and a regular chow. In this study, we employed a low nitrite/nitrate chow in which the contents of those ingredients were identical with the regular chow.

We previously created mice in which all three NOS isoforms are completely disrupted (triply n/i/eNOSs$^{-/-}$ mice) [37], and indicated that both their plasma nitrite/nitrate concentrations and urinary nitrite/nitrate excretion were extremely low, with less than 10% of the normal levels in WT mice [38]. These results suggested that in vivo NO synthesis is predominantly regulated by endogenous NOSs, and that the contribution of the exogenous NO production system to that regulation might be minor. However, contrary to these suggestions, another study showed that a 1-week LND markedly decreased the plasma nitrite/nitrate levels in WT mice bearing normal NOS activities as compared with a RD [21], although its possible mechanisms remain to be clarified.

In this study, we obtained a similar finding that LND for 1.5-4.5 months markedly reduced plasma nitrite/nitrate levels in WT mice. We then examined the mechanisms, and found that the eNOS expression levels in the visceral fat, but not in the aorta, were markedly suppressed in the 3-month LND-fed mice, accounting for the markedly depressed plasma nitrite/nitrate levels induced by the LND. We also found that the adiponectin levels in the visceral fat were remarkably low in the 3-month LND-fed mice. Adiponectin has been reported to up-regulate eNOS [39], so the adiponectin insufficiency may have mediated the visceral adipose eNOS

down-regulation induced by the LND. It has also been reported that eNOS enhances the adiponectin levels in adipocytes [40]. Thus, there may be a vicious cycle of adiponectin insufficiency and eNOS down-regulation, and this vicious cycle may contribute to the markedly diminished plasma nitrite/nitrate levels induced by the LND.

The levels of PPAR-γ, total AMPK, and p-AMPK were significantly lower in the EWAT in the 1-week LND-fed mice as compared with the RD. As it has been reported that PPAR-γ and AMPK increase adiponectin expression levels in adipocytes [41, 42], it is conceivable that reduced PPAR-γ and AMPK in the visceral fat were involved in the adiponectin insufficiency induced by the LND.

The 3-month LND-fed mice exhibited visceral obesity with adipocyte hypertrophy, hyper-LDL and hyper-small dense LDL cholesterolemia, and glucose intolerance, and the 18-month LND-fed mice manifested body weight gain, hypertension, insulin resistance, and endothelial dysfunction. These changes eventually resulted in the occurrence of death due to cardiovascular disease, including acute myocardial infarction. These abnormalities were reversed by concurrent nitrate supplementation, indicating that the observed effects were indeed caused by dietary nitrite/nitrate deficiency. It is thus evident that long-term dietary nitrite/nitrate deficiency causes MetS, endothelial dysfunction, and cardiovascular death in mice. The 3- and 4.5-month LND significantly reduced blood glucose-lowering responses to insulin, but did not significantly affect fasting plasma insulin levels. Thus, prior to 18 months, the effects of LND on glucose tolerance could be due to those on pancreatic beta cell function.

A clustering of cardiovascular risk factors (i.e., MetS) could have contributed to the development of endothelial dysfunction and cardiovascular death in the LND-fed mice. On the other hand, hyper-LDL-cholesterolemia and hyper-small dense LDL-cholesterolemia, both of which are independent cardiovascular risk factors [43], were also noted in the LND-fed mice. The small dense LDL particle can easily

penetrate the vascular wall because of its small particle size, and is related more strongly to the risk of cardiovascular disease. It is thus likely that those factors may also have been independently involved in the occurrence of endothelial dysfunction and cardiovascular death in the LND-fed mice.

The 18-month LND-fed mice displayed an impairment of endothelium-dependent relaxations to acetylcholine, a physiological eNOS activator, along with aortic eNOS down-regulation, suggesting the presence of coronary vasospasm. Coronary vasospasm-elicited myocardial ischaemia can lead to fatal cardiac arrhythmia and/or cardiogenic shock. On the other hand, the dead LND-fed mice showed acute myocardial infarction, myocardial fibrosis which might have resulted from myocardial infarction, and coronary perivascular fibrosis. They also exhibited pulmonary congestion and acute renal tubular necrosis, both of which are seen in cardiac sudden death. Taken together, we though that 83.3% (5/6) of the dead LND-fed mice had been consistent with cardiovascular death.

The data obtained at 3 and 4.5 months are the most important and significant, as the changes in glucose metabolism, lipid biology, body fat distribution, and gut microbiome occurred independent of food intake and body weight. On the other hand, the morbidity and mortality experiments at 18 and 22 months, respectively, are complicated by greater weight gain in the LND group, making it difficult to separate the effects of obesity from nitrite/nitrate deficiency.

We conducted the glucose and insulin tolerance tests under anaesthesia. Whereas it has been reported that high-fat diet-fed C57BL/6J mice show glucose intolerance compared with regular diet-fed counterparts whether they were tested under conscious or anesthetized conditions [44], it has also been indicated that the use of anaesthesia could influence glucose tolerance in C57BL/6J mice [45]. Therefore, the use of anaesthesia could be a limitation of this study.

An increased number of inflammatory foci, decreased eNOS expression levels,

and lower adiponectin levels were noted in the visceral fat of the LND-fed mice, and improvements of the LND-induced MetS by nitrate supplementation were linked to ameliorations of these changes. As it has been reported that inflammation, eNOS down-regulation, and adiponectin insufficiency contribute to the occurrence and progression of MetS [46-48], it is possible that those factors were involved in the development of the MetS induced by the LND.

The following lines of evidence suggest a causal role of gut microbiota dysbiosis in the development of MetS. First, it has been reported that the composition of gut microbiota differs largely between lean individuals and patients with MetS [33]. Secondly, it has been indicated that transplantation of gut microbiota from obese humans with metabolic abnormalities into germ-free mice results in the development of obesity and metabolic abnormalities in the mice [49]. Thirdly, it has been shown that transfer of gut microbiota from lean healthy humans into patients with MetS improves insulin resistance in the patients [33]. In our study, there were significantly fewer operational taxonomic units in the LND than in the RD, suggesting less diversity of gut microbiota in the LND-fed mice. There also were significantly different constituents of gut microbiota in a variety of the hierarchy ranks in the LND and the RD. In agreement with these results, the thirdly-mentioned study above indicated that less diversity and distinct constituents of gut microbiota were recognized in patients with MetS, and that the improvement of insulin resistance after the gut microbiota transfer was accompanied by the amelioration of the reduced diversity and the distinct constituents of gut microbiota [33]. Thus, it is possible that dysbiotic gut microbiota were involved in the pathogenesis of MetS induced by the LND.

We matched the energy contents in the two diets completely, and food consumption was comparable between the LND and RD at 1.5, 3, 4.5 and 18 months after the start of the diet, suggesting similar energy intake in the LND and RD. Nevertheless, the LND-fed mice developed MetS. Therefore, we may have succeeded

for the first time in identifying specific dietary ingredients that cause MetS even in the absence of excessive intake of energy.

In summary, we were able to demonstrate that long-term dietary nitrite/nitrate deficiency gave rise to MetS, endothelial dysfunction, and eventually cardiovascular death in mice, indicating a novel pathogenetic role of the exogenous NO production system in MetS and its vascular complications.

Funding

This work was supported in part by Grant-in-Aids for Research Activity Start-up (15H06519) and Scientific Research (C) (16K09519) from the Japan Society for the Promotion of Science, Special Account Budgets for Education and Research granted by the Japan Ministry of Education, and Grants from the Okinawa Medical Science Research Foundation, from the Ryukyu University Support Foundation, from the Promotion Project of Medical Clustering of Okinawa Prefecture, from the Okinawa Prefecture for Promotion of Advanced Medicine, and from the University of the Ryukyus, Japan.

Author Contributions

M.K-T. and M.S. designed the study, acquired, analysed, and interpreted data, drafted and revised the article, and approved the final version. A.T. acquired, analysed, and interpreted data, drafted the article, and approved the final version. T.K., T.M., N.K., T.U., J.N., C.K., M.I., H.K., Y.Taira., Y.Totsuka., S.K., J.O. and K.S. acquired, analysed, and interpreted data, and approved the final version. H.Sunakawa and H.M. designed the study, analysed and interpreted data, and approved the final version. H.Shimokawa, N.Y., S.M., Y.O., M.M. and A.A. analysed and interpreted data and approved the final version. M.T. designed the study, analysed, and interpreted data, drafted and revised the article, and approved the final version. M.T. is the guarantor of this work.

Duality of Interest

The authors declare that there is no duality of interest associated with this manuscript.

References

[1] Eckel R (2015) The Metabolic Syndrome. In: Kasper DL, Fauci AS, Hauser SL, Longo DL, Jameson JL, Loscaldo J (eds) Harrison's Principles of Internal Medicine. Mc Graw Hill Education, New York, pp 2449-2454

[2] Beltran-Sanchez H, Harhay MO, Harhay MM, McElligott S (2013) Prevalence and trends of metabolic syndrome in the adult U.S. population, 1999-2010. J Am Coll Cardiol 62: 697-703

[3] Alberti KG, Eckel RH, Grundy SM, et al. (2009) Harmonizing the metabolic syndrome: a joint interim statement of the International Diabetes Federation Task Force on Epidemiology and Prevention; National Heart, Lung, and Blood Institute; American Heart Association; World Heart Federation; International Atherosclerosis Society; and International Association for the Study of Obesity. Circulation 120: 1640-1645

[4] Mottillo S, Filion KB, Genest J, et al. (2010) The metabolic syndrome and cardiovascular risk a systematic review and meta-analysis. J Am Coll Cardiol 56: 1113-1132

[5] Chen J, Muntner P, Hamm LL, et al. (2004) The metabolic syndrome and chronic kidney disease in U.S. adults. Ann Intern Med 140: 167-174

[6] Esposito K, Chiodini P, Colao A, Lenzi A, Giugliano D (2012) Metabolic syndrome and risk of cancer: a systematic review and meta-analysis. Diabetes Care 35: 2402-2411

[7] Garg PK, Biggs ML, Carnethon M, et al. (2014) Metabolic syndrome and risk of incident peripheral artery disease: the cardiovascular health study. Hypertension 63: 413-419

[8] Hamaguchi M, Kojima T, Takeda N, et al. (2005) The metabolic syndrome as a predictor of nonalcoholic fatty liver disease. Ann Intern Med 143: 722-728

[9] Hanley AJ, Karter AJ, Williams K, et al. (2005) Prediction of type 2 diabetes mellitus with alternative definitions of the metabolic syndrome: the Insulin Resistance Atherosclerosis Study. Circulation 112: 3713-3721

[10] Ignarro LJ (1990) Biosynthesis and metabolism of endothelium-derived nitric oxide. Annu Rev Pharmacol Toxicol 30: 535-560

[11] Moncada S, Higgs A (1993) The L-arginine-nitric oxide pathway. N Engl J Med 329: 2002-2012

[12] Murad F (2006) Shattuck Lecture. Nitric oxide and cyclic GMP in cell signaling and drug development. N Engl J Med 355: 2003-2011

[13] Tsutsui M, Shimokawa H, Otsuji Y, Yanagihara N (2010) Pathophysiological relevance of NO signaling in the cardiovascular system: novel insight from mice lacking all NO synthases. Pharmacol Ther 128: 499-508

[14] Tsutsui M, Shimokawa H, Tanimoto A, Yanagihara N, Otsuji Y (2014) Roles of nitric oxide synthases in arteriosclerotic vascular disease - Insights from murine genetic models -. J Clin Exp Cardiol 5: 318. doi:310.4172/2155-9880.1000318

[15] Tsutsui M, Tanimoto A, Tamura M, et al. (2015) Significance of nitric oxide synthases: Lessons from triple nitric oxide synthases null mice. J Pharmacol Sci 127: 42-52

[16] Kevil CG, Lefer DJ (2011) Review focus on inorganic nitrite and nitrate in cardiovascular health and disease. Cardiovasc Res 89: 489-491

[17] Lundberg JO, Weitzberg E, Gladwin MT (2008) The nitrate-nitrite-nitric oxide pathway in physiology and therapeutics. Nat Rev Drug Discov 7: 156-167

[18] Omar SA, Webb AJ (2014) Nitrite reduction and cardiovascular protection. J Mol Cell Cardiol 73: 57-69

[19] Milkowski A, Garg HK, Coughlin JR, Bryan NS (2010) Nutritional epidemiology in the context of nitric oxide biology: a risk-benefit evaluation for dietary nitrite and nitrate. Nitric Oxide 22: 110-119

[20] Weitzberg E, Lundberg JO (2013) Novel aspects of dietary nitrate and human health. Annu Rev Nutr 33: 129-159

[21] Bryan NS, Calvert JW, Elrod JW, Gundewar S, Ji SY, Lefer DJ (2007) Dietary nitrite supplementation protects against myocardial ischemia-reperfusion injury. Proc Natl Acad Sci U S A 104: 19144-19149

[22] Bryan NS, Calvert JW, Gundewar S, Lefer DJ (2008) Dietary nitrite restores NO homeostasis and is cardioprotective in endothelial nitric oxide synthase-deficient mice. Free Radic Biol Med 45: 468-474

[23] Zhan J, Nakao A, Sugimoto R, et al. (2009) Orally administered nitrite attenuates cardiac allograft rejection in rats. Surgery 146: 155-165

[24] Park JW, Piknova B, Huang PL, Noguchi CT, Schechter AN (2013) Effect of blood nitrite and nitrate levels on murine platelet function. PLoS One 8: e55699

[25] Usui S, Hara Y, Hosaki S, Okazaki M (2002) A new on-line dual enzymatic method for simultaneous quantification of cholesterol and triglycerides in lipoproteins by HPLC. J Lipid Res 43: 805-814

[26] Uchida T, Furuno Y, Tanimoto A, et al. (2014) Development of an experimentally useful model of acute myocardial infarction: 2/3 nephrectomized triple nitric oxide synthases-deficient mouse. J Mol Cell Cardiol 77: 29-41

[27] Satoh K, Satoh T, Kikuchi N, et al. (2014) Basigin mediates pulmonary hypertension by promoting inflammation and vascular smooth muscle cell proliferation. Circ Res 115: 738-750

[28] Kim SW, Suda W, Kim S, et al. (2013) Robustness of gut microbiota of healthy adults in response to probiotic intervention revealed by high-throughput pyrosequencing. DNA Res 20: 241-253

[29] Qin N, Yang F, Li A, et al. (2014) Alterations of the human gut microbiome in liver cirrhosis. Nature 513: 59-64

[30] Lecomte V, Kaakoush NO, Maloney CA, et al. (2015) Changes in gut microbiota

in rats fed a high fat diet correlate with obesity-associated metabolic parameters. PLoS One 10: e0126931

[31] Ley RE, Backhed F, Turnbaugh P, Lozupone CA, Knight RD, Gordon JI (2005) Obesity alters gut microbial ecology. Proc Natl Acad Sci U S A 102: 11070-11075

[32] Turnbaugh PJ, Ley RE, Mahowald MA, Magrini V, Mardis ER, Gordon JI (2006) An obesity-associated gut microbiome with increased capacity for energy harvest. Nature 444: 1027-1031

[33] Vrieze A, Van Nood E, Holleman F, et al. (2012) Transfer of intestinal microbiota from lean donors increases insulin sensitivity in individuals with metabolic syndrome. Gastroenterology 143: 913-916 e917

[34] Everard A, Belzer C, Geurts L, et al. (2013) Cross-talk between Akkermansia muciniphila and intestinal epithelium controls diet-induced obesity. Proc Natl Acad Sci U S A 110: 9066-9071

[35] Shin NR, Lee JC, Lee HY, et al. (2014) An increase in the Akkermansia spp. population induced by metformin treatment improves glucose homeostasis in diet-induced obese mice. Gut 63: 727-735

[36] Gauffin Cano P, Santacruz A, Moya A, Sanz Y (2012) Bacteroides uniformis CECT 7771 ameliorates metabolic and immunological dysfunction in mice with high-fat-diet induced obesity. PLoS One 7: e41079

[37] Morishita T, Tsutsui M, Shimokawa H, et al. (2005) Nephrogenic diabetes insipidus in mice lacking all nitric oxide synthase isoforms. Proc Natl Acad Sci U S A 102: 10616-10621

[38] Nakata S, Tsutsui M, Shimokawa H, et al. (2008) Spontaneous myocardial infarction in mice lacking all nitric oxide synthase isoforms. Circulation 117: 2211-2223

[39] Hattori Y, Suzuki M, Hattori S, Kasai K (2003) Globular adiponectin upregulates nitric oxide production in vascular endothelial cells. Diabetologia 46: 1543-1549

[40] Koh EH, Kim M, Ranjan KC, et al. (2010) eNOS plays a major role in adiponectin synthesis in adipocytes. Am J Physiol Endocrinol Metab 298: E846-853

[41] Bouskila M, Pajvani UB, Scherer PE (2005) Adiponectin: a relevant player in PPARgamma-agonist-mediated improvements in hepatic insulin sensitivity? Int J Obes 29 Suppl 1: S17-23

[42] Daval M, Foufelle F, Ferre P (2006) Functions of AMP-activated protein kinase in adipose tissue. J Physiol 574: 55-62

[43] Sniderman AD, Furberg CD, Keech A, et al. (2003) Apolipoproteins versus lipids as indices of coronary risk and as targets for statin treatment. Lancet 361: 777-780

[44] Andrikopoulos S, Blair AR, Deluca N, Fam BC, Proietto J (2008) Evaluating the glucose tolerance test in mice. Am J Physiol Endocrinol Metab 295: E1323-1332

[45] Windelov JA, Pedersen J, Holst JJ (2016) Use of anesthesia dramatically alters the oral glucose tolerance and insulin secretion in C57Bl/6 mice. Physiol Rep 4: e12824

[46] Duplain H, Burcelin R, Sartori C, et al. (2001) Insulin resistance, hyperlipidemia, and hypertension in mice lacking endothelial nitric oxide synthase. Circulation 104: 342-345

[47] Matsuzawa Y, Funahashi T, Kihara S, Shimomura I (2004) Adiponectin and metabolic syndrome. Arterioscler Thromb Vasc Biol 24: 29-33

[48] Romeo GR, Lee J, Shoelson SE (2012) Metabolic syndrome, insulin resistance, and roles of inflammation - mechanisms and therapeutic targets. Arterioscler Thromb Vasc Biol 32: 1771-1776

[49] Ridaura VK, Faith JJ, Rey FE, et al. (2013) Gut microbiota from twins discordant for obesity modulate metabolism in mice. Science 341: 1241214

Table 1. Composition of regular chow and low nitrite/nitrate chow

	Regular chow	**Low nitrite/nitrate chow**
Protein (%kJ)	28.5	28.5
Fat (%kJ)	13.5	13.5
Carbohydrate (%kJ)	58.0	58.0
L-arginine (g/kg)	14.1	14.1
Nitrite (μmol/kg)	< 6.5	< 6.5
Nitrate (μmol/kg)	548.3	< 4.8

Values are expressed as mean values of two samples.

Table 2. Nitrate and nitrite levels in tap and ultrapure water

	Tap water	**Ultrapure water**
Nitrite (μmol/l)	3.30	< 0.01
Nitrate (μmol/l)	6.07	< 0.01

Values are expressed as mean values of two samples.

Table 3. Plasma triacylglycerol levels at 1.5, 3, and 4.5 months after the start of RD or LND

Diet	Plasma triacylglycerol levels (mmol/l)		
	1.5 months	3 months	4.5 months
RD (n=6-12)	1.23 ± 0.07	0.94 ± 0.05	1.06 ± 0.07
LND (n=6-12)	1.25 ± 0.07	1.41 ± 0.19	1.21 ± 0.19

Statistical analysis was performed by two-way factorial ANOVA followed by Bonferroni's *post hoc* test for multiple comparisons, and no significant differences were seen.

Table 4. Serum levels of 23 inflammatory markers in mice fed RD and LND for 1.5 months

	Serum levels (pg/ml) (n=8-10)		*p* value
	RD	LND	
IL-1α	31.3 ± 4.5	28.0 ± 3.0	0.55
IL-1β	643.9 ± 67.2	558.5 ± 72.1	0.40
IL-2	110.4 ± 18.2	93.4 ± 19.2	0.54
IL-3	27.5 ± 4.6	23.5 ± 4.2	0.53
IL-4	51.7 ± 8.3	46.6 ± 9.3	0.69
IL-5	89.5 ± 14.2	72.8 ± 13.1	0.40
IL-6	67.3 ± 8.6	55.7 ± 8.3	0.34
IL-9	580.2 ± 54.8	544.4 ± 33.7	0.60
IL-10	217.9 ± 56.5	134.3 ± 23.4	0.19
IL-12p40	459.1 ± 26.7	401.8 ± 31.3	0.18
IL-12p70	1084.5 ± 118.6	800.0 ± 139.3	0.14
IL-13	724.3 ± 104.6	714.4 ± 108.3	0.95
IL-17	342.7 ± 30.0	275.5 ± 30.2	0.13
TNF-α	847.6 ± 103.5	632.7 ± 107.4	0.17
IFN-γ	111.6 ± 14.5	85.7 ± 15.7	0.24
MCP-1	746.2 ± 72.7	590.0 ± 70.2	0.14
MIP-1α	74.4 ± 8.4	59.0 ± 10.0	0.26
MIP-1β	131.6 ± 19.0	105.1 ± 16.8	0.31
G-CSF	184.7 ± 22.4	128.6 ± 18.2	0.07
GM-CSF	456.9 ± 19.2	437.8 ± 25.7	0.56
KC	137.6 ± 16.9	118.7 ± 8.1	0.33
Eotaxin	1459.7 ± 75.0	1397.2 ± 104.0	0.63
RANTES	34.2 ± 2.2	23.4 ± 1.3	0.0004

IL, interleukin; TNF, tumour necrosis factor; IFN, interferon; MCP, monocyte chemotactic protein; MIP, macrophage inflammatory protein; G-CSF, granulocyte-colony stimulating factor; GM-CSF, granulocyte/macrophage-colony stimulating factor; KC, keratinocyte-derived chemokine; RANTES, regulated on activation normal cell expressed and secreted.

Figure Legends

Fig. 1

Effects of 1.5-4.5 months of LND on plasma nitrite/nitrate, eNOS expression, food intake, and visceral fat in WT mice. **a**, Plasma nitrite/nitrate levels (n=8-12). White bars; RD, black bars; LND. **b**,**c**, eNOS protein levels in the aorta (n=6) and EWAT induced by 3 months of LND (n=10). **d**,**e**, Food intake (n=10-12) and EWAT-to-body weight (n=10-12). White bars; RD, black bars; LND. **f**, Epididymal white adipocyte size induced by 3 months of LND (n=10). Scale bars=50 μm. *p<0.05, **p<0.01, and ***p<0.001.

Fig. 2

Effects of 1.5-4.5 months of LND on plasma lipid, blood glucose, and insulin response. **a**, Plasma total cholesterol levels (n=10-12). White bars; RD, black bars; LND. **b**, Plasma LDL cholesterol levels induced by 3 months of LND (n=12). **c-e**, Blood glucose levels after intraperitoneal injection of 1 g/kg glucose after 1.5 (**c**), 3 (**d**), and 4.5 (**e**) months of LND (n=11-12). White circles; RD, black squares; LND. **f-h**, Percent change of blood glucose levels after intraperitoneal injection of 0.3 unit/kg insulin after 1.5 (**f**), 3 (**g**), and 4.5 (**h**) months of LND (n=8-12). White circles; RD, black squares; LND. *p<0.05, **p<0.01, and ***p<0.001.

Fig. 3

Effects of 3 months of LND on adiponectin and effects of 1 week of LND on PPAR-γ, total AMPK, phosphorylated AMPK (p-AMPK), and sirtuin1 levels in the EWAT. **a**, Adiponectin levels (n=5). **b-e**, PPAR-γ, total AMPK, p-AMPK, and sirtuin1 levels (n=7). *p<0.05, **p<0.01, and ***p<0.001.

Fig. 4

Effects of 3 months of nitrate supplementation on MetS-like conditions induced by LND. **a**, Plasma nitrite/nitrate levels (n=6-12). **b**, EWAT-to-body weight (n=7-8). **c**, Epididymal white adipocyte size (n=10). Scale bars=50 μm. **d**, Plasma small dense LDL cholesterol levels (n=10-12). **e**, Blood glucose levels after intraperitoneal injection of 1 g/kg glucose (n=8). Black squares; LND, white triangles; LND + Nitrate. **f**, Percent change of blood glucose levels after intraperitoneal injection of 0.3 unit/kg insulin (n=9-10). Black squares; LND, white triangles; LND + Nitrate. **g**,**h,** eNOS (n=5-6) and adiponectin levels (n=3) in the EWAT. *p<0.05, **p<0.01, and ***p<0.001.

Fig. 5

Effects of 3 months of LND on gut microbiota. **a**, Operational taxonomic units (n=5 each). **b,c**, Significantly higher (**b**) or lower (**c**) gut bacteria in the genus rank (p<0.05, n=5 each). White boxes; RD, grey boxes; LND. Insets are the magnified views of sequencing reads of the rightmost three gut bacteria in panels **b** and **c**. *p<0.05.

Fig. 6

Effects of 18 months of LND and nitrate supplementation on body weight, body fat, plasma small dense LDL, blood glucose, and insulin sensitivity. **a**, Body weight (n=12-16). **b**, Micro-CT images. **c**, Body fat-to-body mass (n=11-12). **d**, Visceral fat-to-body mass (n=11-12). **e**, Plasma small dense LDL cholesterol levels (n=7-9). **f**, Blood glucose levels after intraperitoneal injection of 1 g/kg glucose (n=12-14). White circles; RD, black squares; LND, white triangles; LND + Nitrate. **g**, Percent change of blood glucose levels after intraperitoneal injection of 0.3 unit/kg insulin (n=10). White circles; RD, black squares; LND, white triangles; LND + Nitrate. *p<0.05 and ***p<0.001 in RD vs. LND; †p<0.05 and ††p<0.01 in LND vs. LND + Nitrate.

Fig. 7

Effects of 18 months of LND and nitrate supplementation on fasting blood glucose, blood pressure, vascular reactivity, eNOS expression, and inflammation. **a**, Fasting blood glucose levels (n=12-14). **b**, Fasting plasma insulin levels (n=6-7). **c**, Systolic blood pressure (n=12-15). **d**, Endothelium-dependent relaxations to ACh (n=6). White circles; RD, black squares; LND, white triangles; LND + Nitrate. **e**, eNOS protein levels in the aorta (n=6). **f,g,** Number of inflammatory foci in the EWAT and the peri-renal WAT (n=12-14). *p<0.05 and ***p<0.001 in RD vs. LND; †p<0.05, ††p<0.01, and †††p<0.001 in LND vs. LND + Nitrate.

Fig. 8

Effects of 22 months of LND and nitrate supplementation on survival rate and postmortem findings in the dead LND-fed mice. **a**, Survival rate (n=15-24). Grey line; RD, black solid line; LND, black dotted line; LND + Nitrate. **b**, Acute myocardial infarction. **c**, Myocardial fibrosis. **d**, Coronary perivascular fibrosis. **e**, Pulmonary congestion. **f**, Acute renal tubular necrosis. **g**, Malignant lymphoma. Scale bars=100 μm.

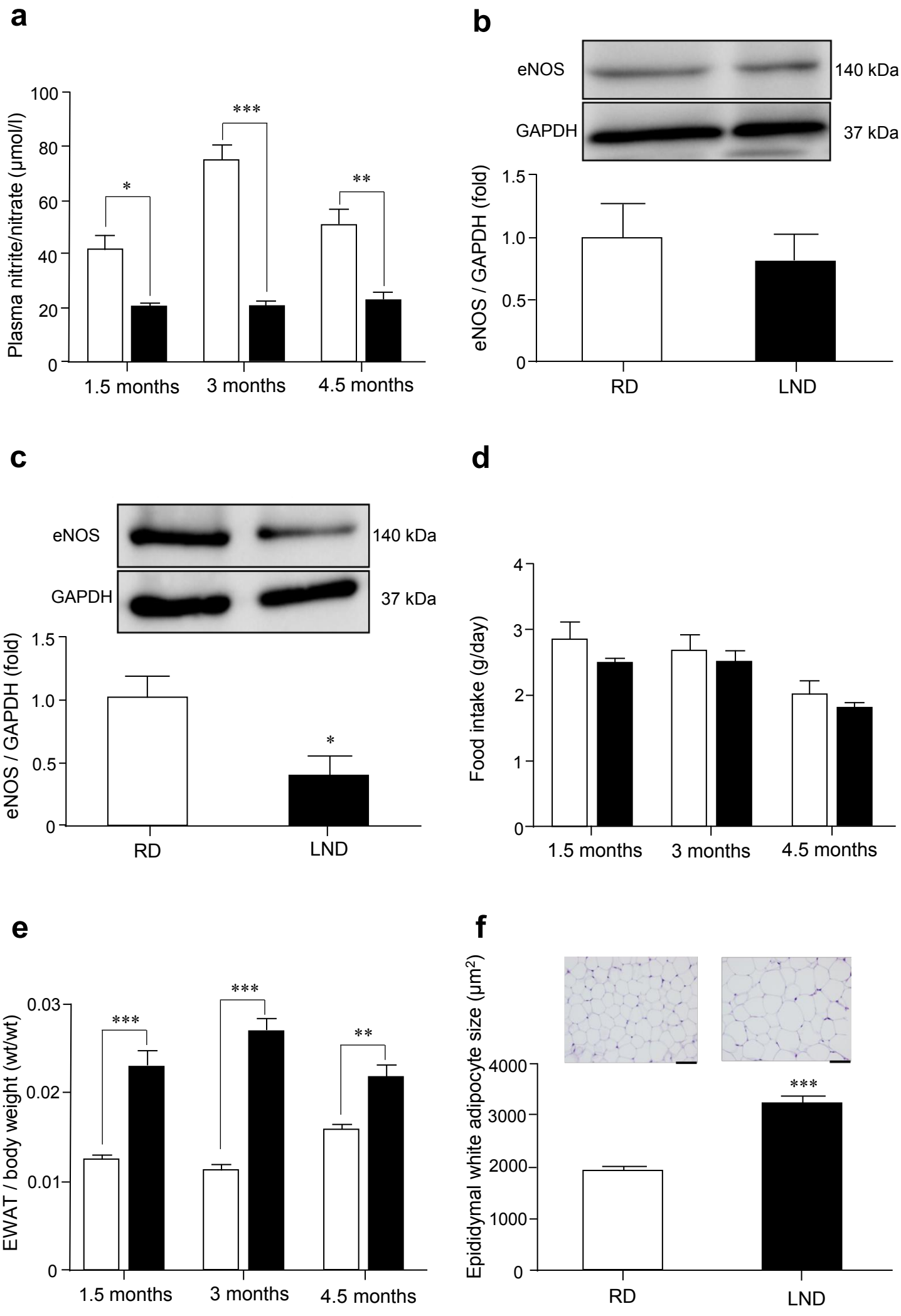
a
Plasma nitrite/nitrate (µmol/l)
100
80
60
40
20
0
*
***
**
1.5 months
3 months
4.5 months
b
eNOS
140 kDa
GAPDH
37 kDa
eNOS / GAPDH (fold)
1.5
1.0
0.5
0
RD
LND
c
eNOS
140 kDa
GAPDH
37 kDa
eNOS / GAPDH (fold)
1.5
1.0
0.5
0
*
RD
LND
d
Food intake (g/day)
4
3
2
1
0
1.5 months
3 months
4.5 months
e
EWAT / body weight (wt/wt)
0.03
0.02
0.01
0
***
***
**
1.5 months
3 months
4.5 months
f
Epididymal white adipocyte size (µm²)
4000
3000
2000
1000
0
***
RD
LND

Fig. 1

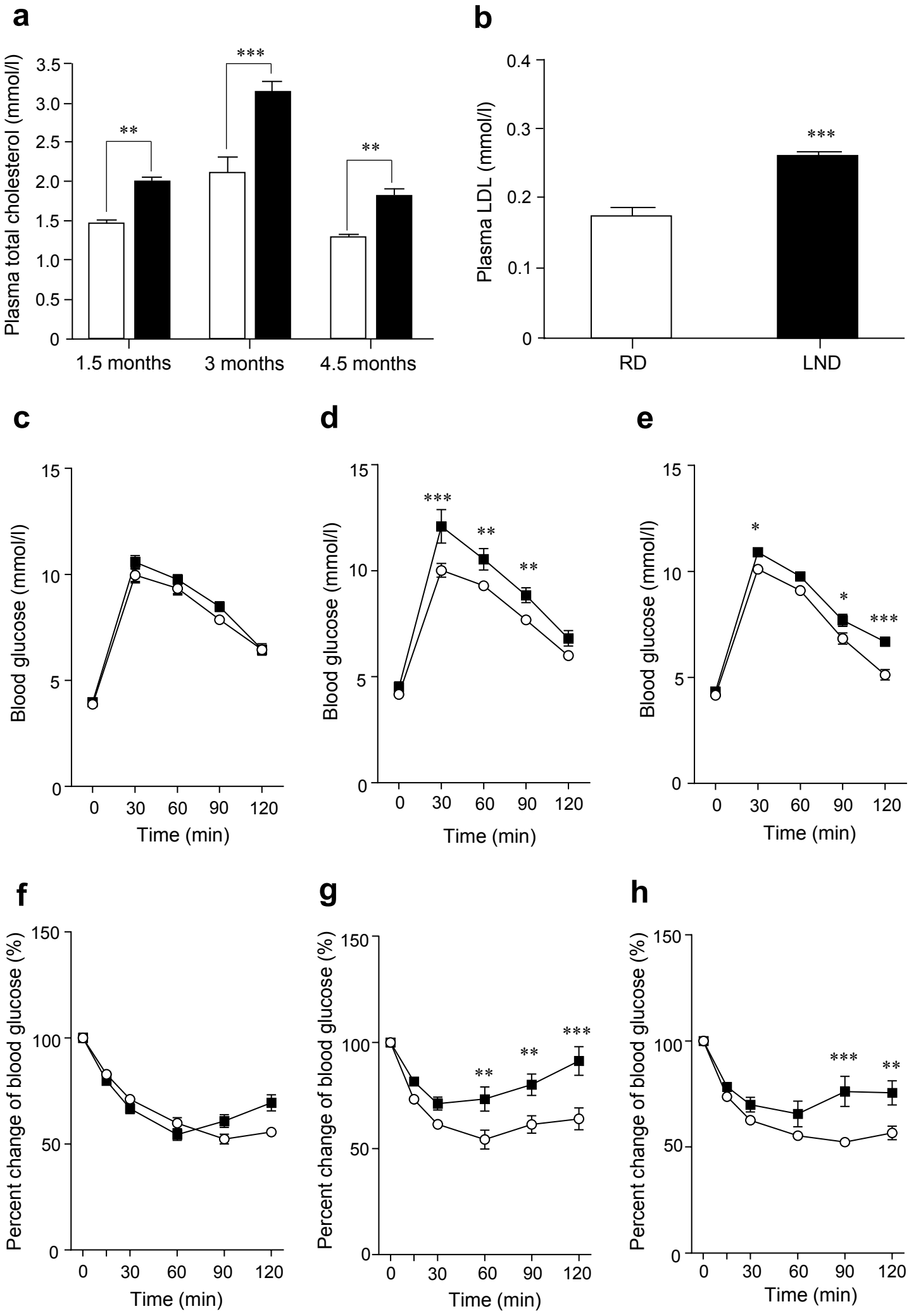
a
Plasma total cholesterol (mmol/l)
3.5
3.0
2.5
2.0
1.5
1.0
0.5
0
**
***
**
1.5 months
3 months
4.5 months
b
Plasma LDL (mmol/l)
0.4
0.3
0.2
0.1
0
***
RD
LND
c
d
e
Blood glucose (mmol/l)
15
10
5
0
0
30
60
90
120
Time (min)
***
**
**
*
*
***
f
g
h
Percent change of blood glucose (%)
150
100
50
0
**
**
***
***
**

Fig. 2

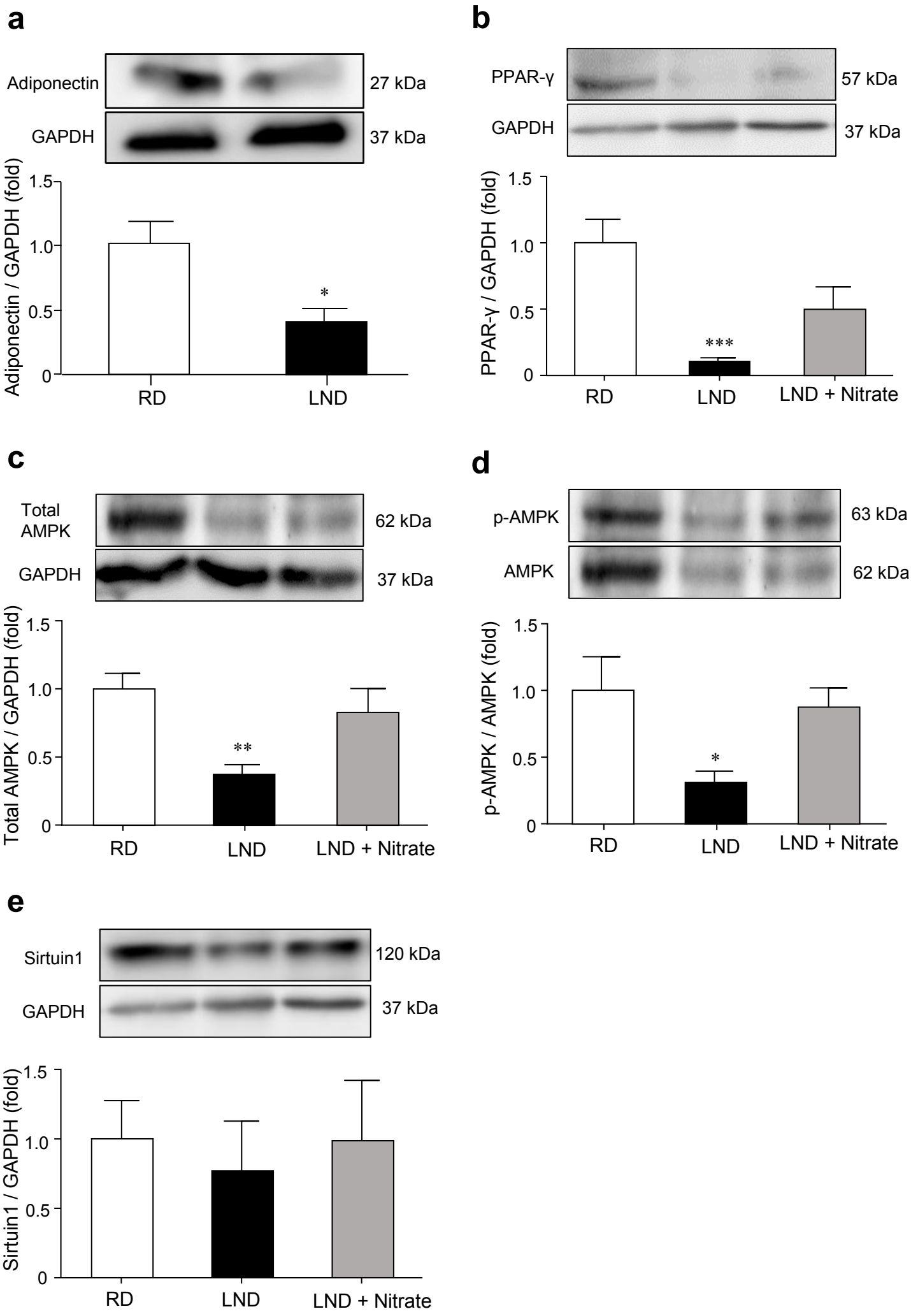
a
Adiponectin
27 kDa
GAPDH
37 kDa
Adiponectin / GAPDH (fold)
1.5
1.0
0.5
0
*
RD
LND
b
PPAR-γ
57 kDa
GAPDH
37 kDa
PPAR-γ / GAPDH (fold)
1.5
1.0
0.5
0
***
RD
LND
LND + Nitrate
c
Total AMPK
62 kDa
GAPDH
37 kDa
Total AMPK / GAPDH (fold)
1.5
1.0
0.5
0
**
RD
LND
LND + Nitrate
d
p-AMPK
63 kDa
AMPK
62 kDa
p-AMPK / AMPK (fold)
1.5
1.0
0.5
0
*
RD
LND
LND + Nitrate
e
Sirtuin1
120 kDa
GAPDH
37 kDa
Sirtuin1 / GAPDH (fold)
1.5
1.0
0.5
0
RD
LND
LND + Nitrate

Fig. 3

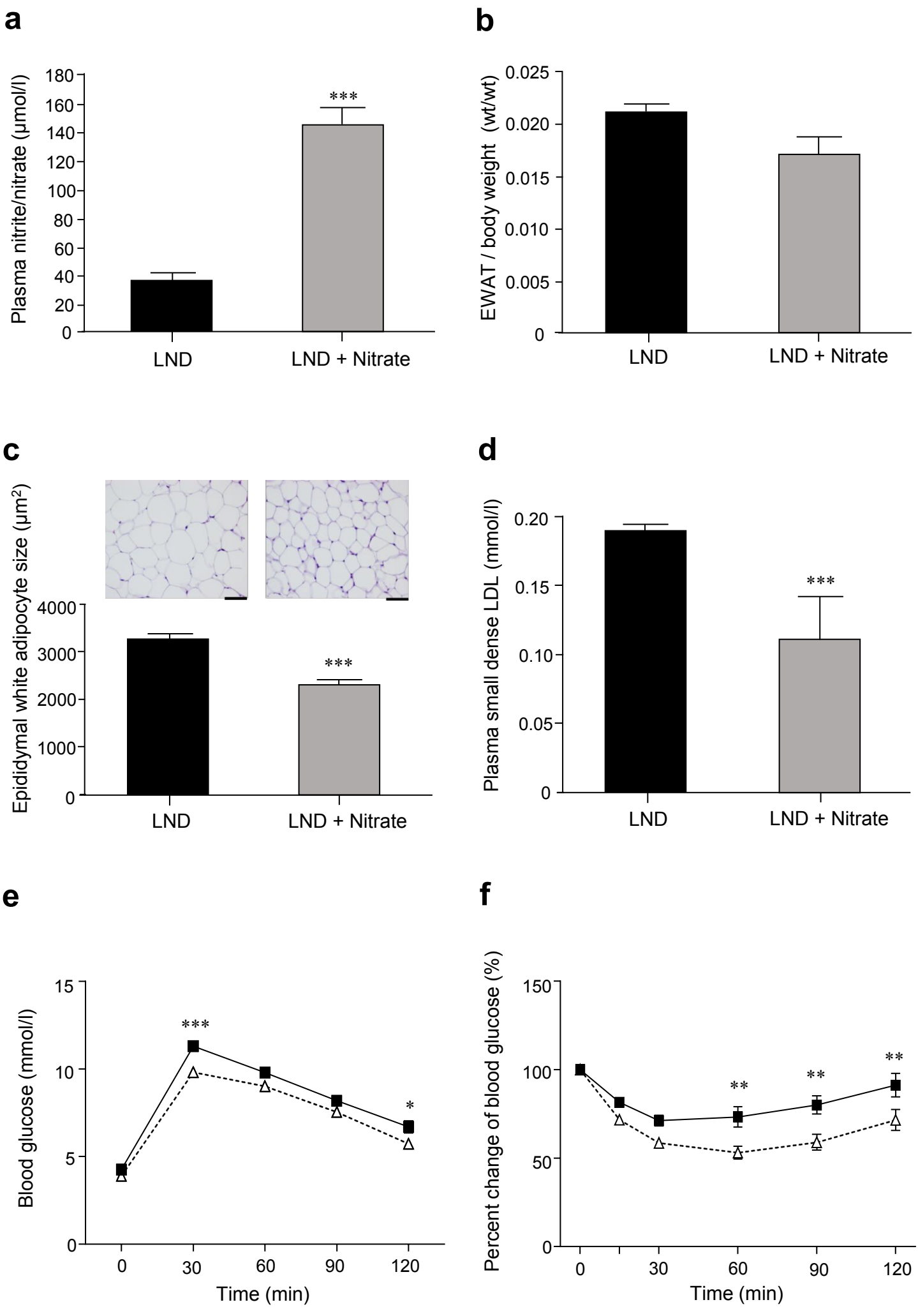
a
Plasma nitrite/nitrate (µmol/l)
180
160
140
120
100
80
60
40
20
0
***
LND
LND + Nitrate
b
EWAT / body weight (wt/wt)
0.025
0.020
0.015
0.010
0.005
0
LND
LND + Nitrate
c
Epididymal white adipocyte size (µm²)
4000
3000
2000
1000
0
***
LND
LND + Nitrate
d
Plasma small dense LDL (mmol/l)
0.20
0.15
0.10
0.05
0
***
LND
LND + Nitrate
e
Blood glucose (mmol/l)
15
10
5
0
***
*
0
30
60
90
120
Time (min)
f
Percent change of blood glucose (%)
150
100
50
0
**
**
**
0
30
60
90
120
Time (min)

Fig. 4 a-f

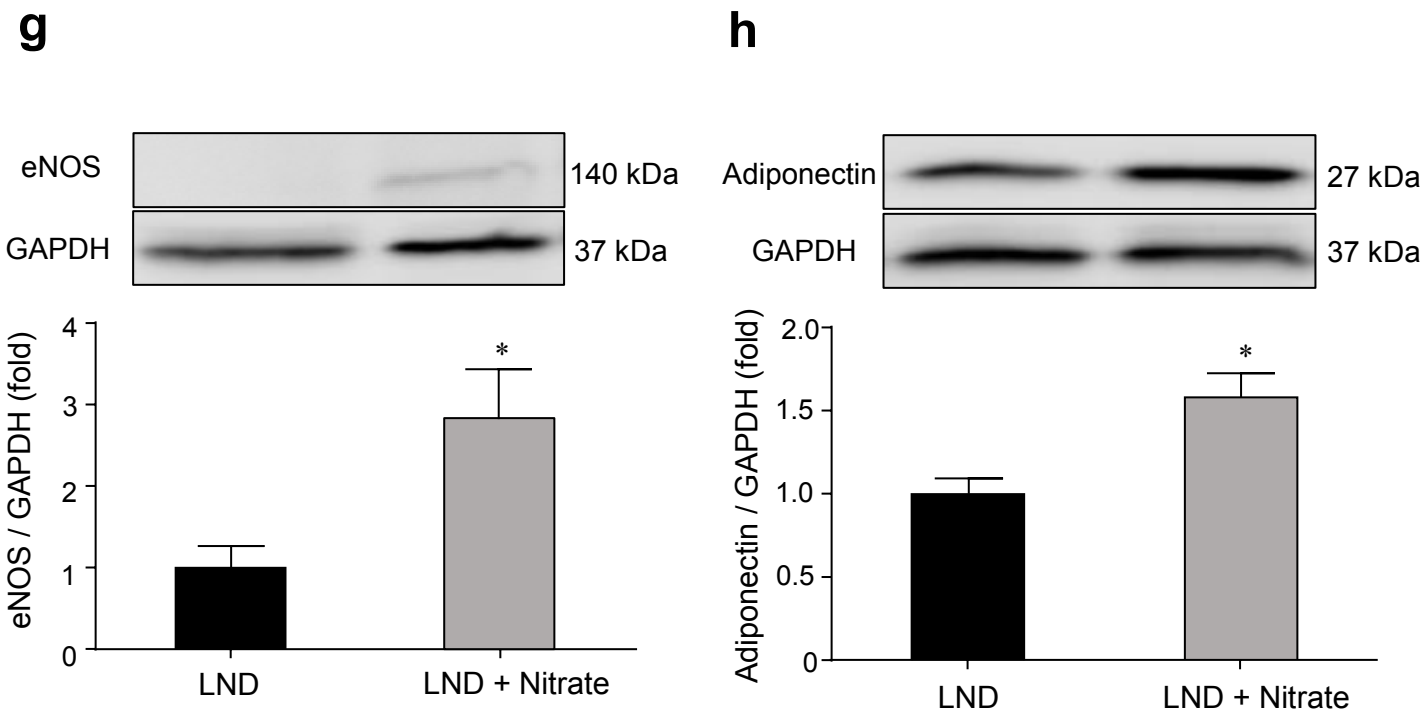
g
eNOS
140 kDa
GAPDH
37 kDa
eNOS / GAPDH (fold)
4
3
2
1
0
*
LND
LND + Nitrate
h
Adiponectin
27 kDa
GAPDH
37 kDa
Adiponectin / GAPDH (fold)
2.0
1.5
1.0
0.5
0
*
LND
LND + Nitrate

Fig. 4 g,h

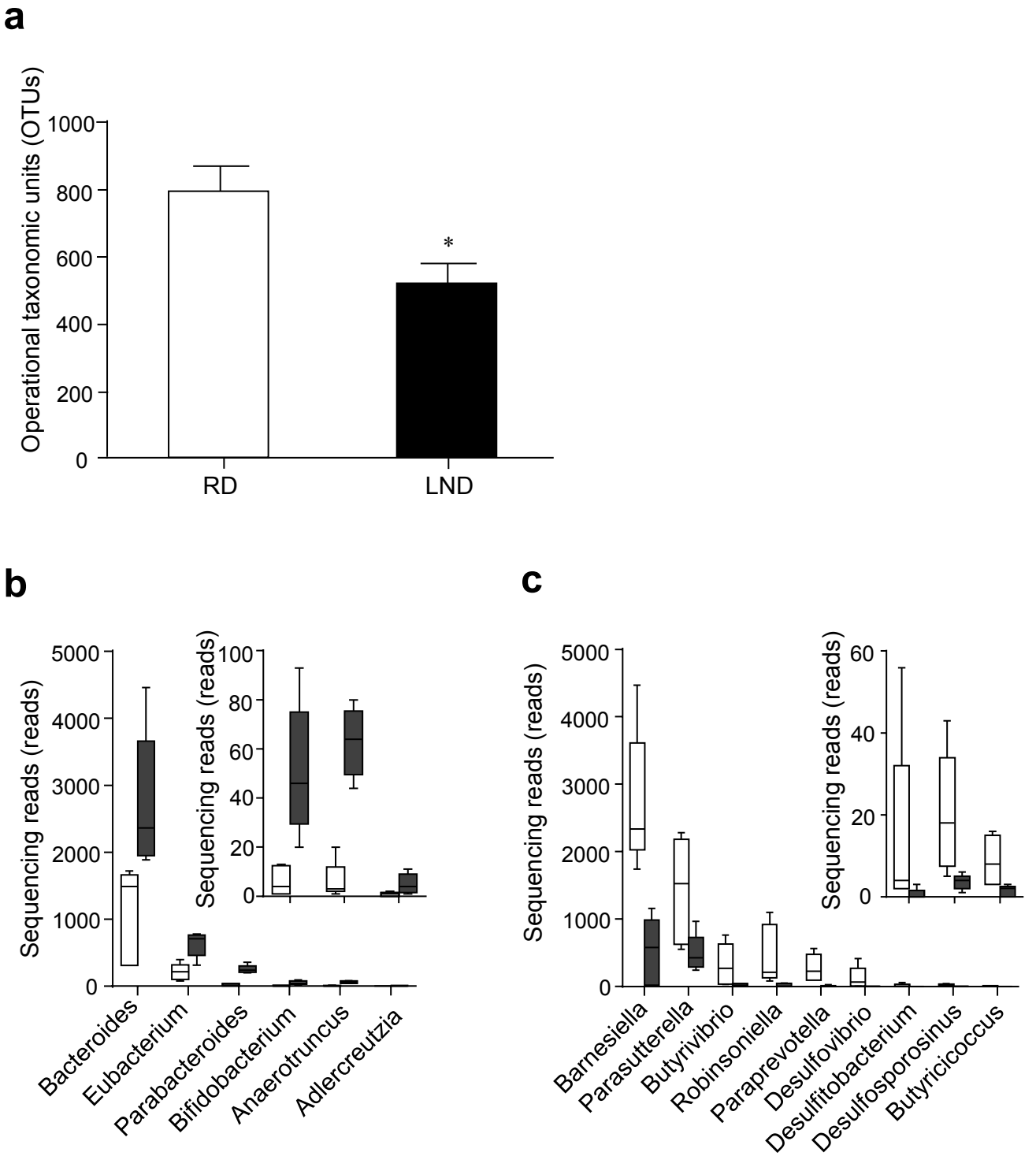
a
Operational taxonomic units (OTUs)
1000
800
600
400
200
0
*
RD
LND
b
Sequencing reads (reads)
5000
4000
3000
2000
1000
0
100
80
60
40
20
0
Bacteroides
Eubacterium
Parabacteroides
Bifidobacterium
Anaerotruncus
Adlercreutzia
c
Sequencing reads (reads)
5000
4000
3000
2000
1000
0
60
40
20
0
Barnesiella
Parasutterella
Butyrivibrio
Robinsoniella
Paraprevotella
Desulfovibrio
Desulfitobacterium
Desulfosporosinus
Butyricicoccus

Fig. 5

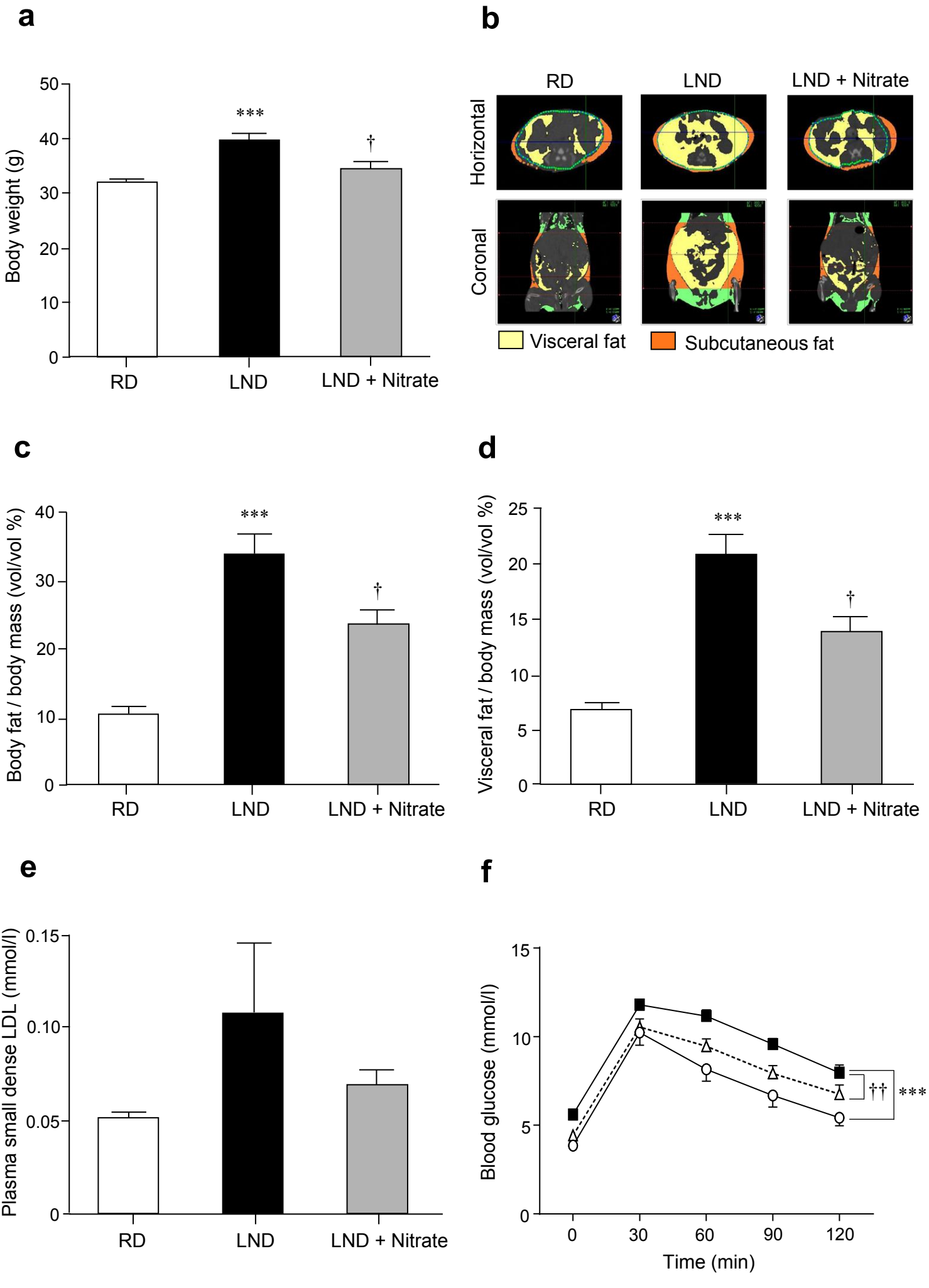
a
Body weight (g)
50
40
30
20
10
0
***
†
RD
LND
LND + Nitrate
b
RD
LND
LND + Nitrate
Horizontal
Coronal
Visceral fat
Subcutaneous fat
c
Body fat / body mass (vol/vol %)
40
30
20
10
0
***
†
RD
LND
LND + Nitrate
d
Visceral fat / body mass (vol/vol %)
25
20
15
10
5
0
***
†
RD
LND
LND + Nitrate
e
Plasma small dense LDL (mmol/l)
0.15
0.10
0.05
0
RD
LND
LND + Nitrate
f
Blood glucose (mmol/l)
15
10
5
0
0
30
60
90
120
Time (min)
††
***

Fig. 6 a-f

g

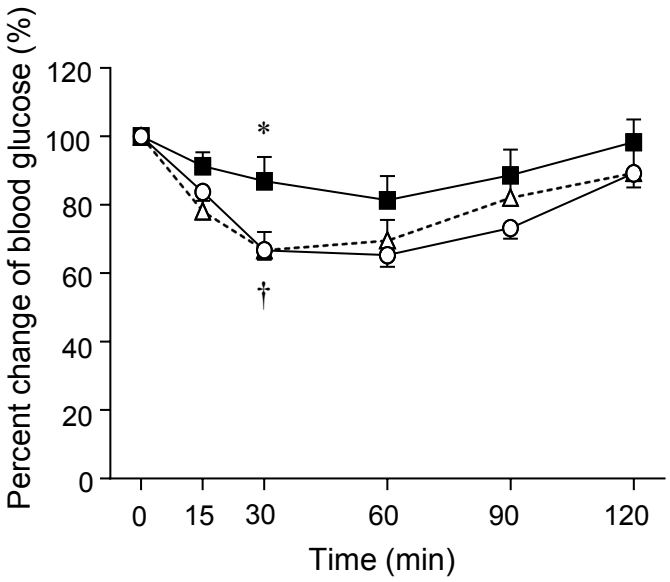
Percent change of blood glucose (%)
120
100
80
60
40
20
0
*
†
0
15
30
60
90
120
Time (min)

Fig. 6 g

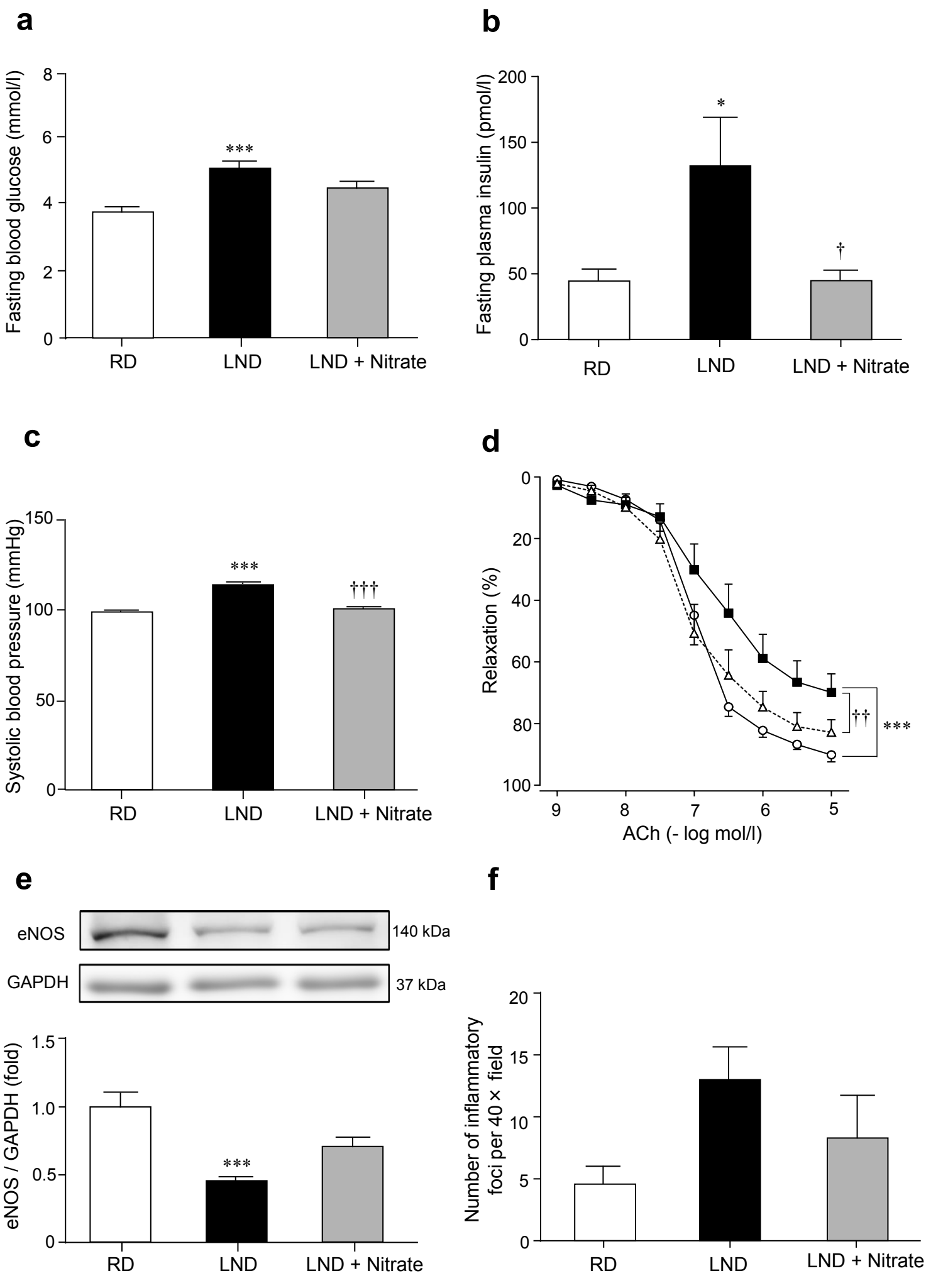
a
Fasting blood glucose (mmol/l)
8
6
4
2
0
***
RD
LND
LND + Nitrate
b
Fasting plasma insulin (pmol/l)
200
150
100
50
0
*
†
RD
LND
LND + Nitrate
c
Systolic blood pressure (mmHg)
150
100
50
0
***
†††
RD
LND
LND + Nitrate
d
Relaxation (%)
0
20
40
60
80
100
9
8
7
6
5
ACh (- log mol/l)
††
***
e
eNOS
140 kDa
GAPDH
37 kDa
eNOS / GAPDH (fold)
1.5
1.0
0.5
0
***
RD
LND
LND + Nitrate
f
Number of inflammatory foci per 40 × field
20
15
10
5
0
RD
LND
LND + Nitrate

Fig. 7 a-f

g

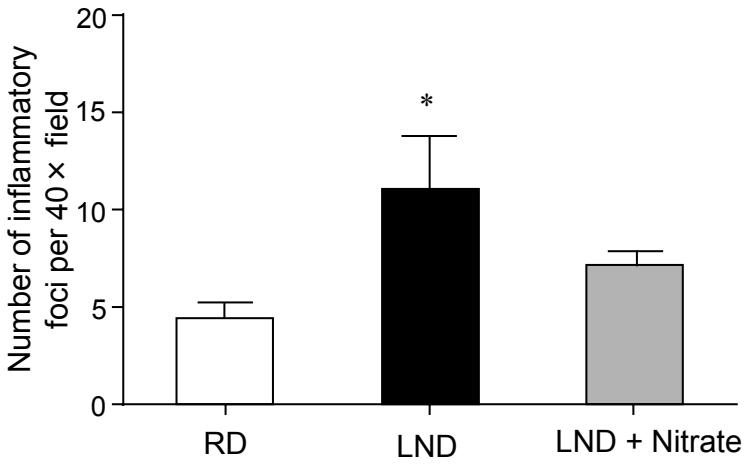
Number of inflammatory foci per 40 × field
20
15
10
5
0
*
RD
LND
LND + Nitrate

Fig. 7 g

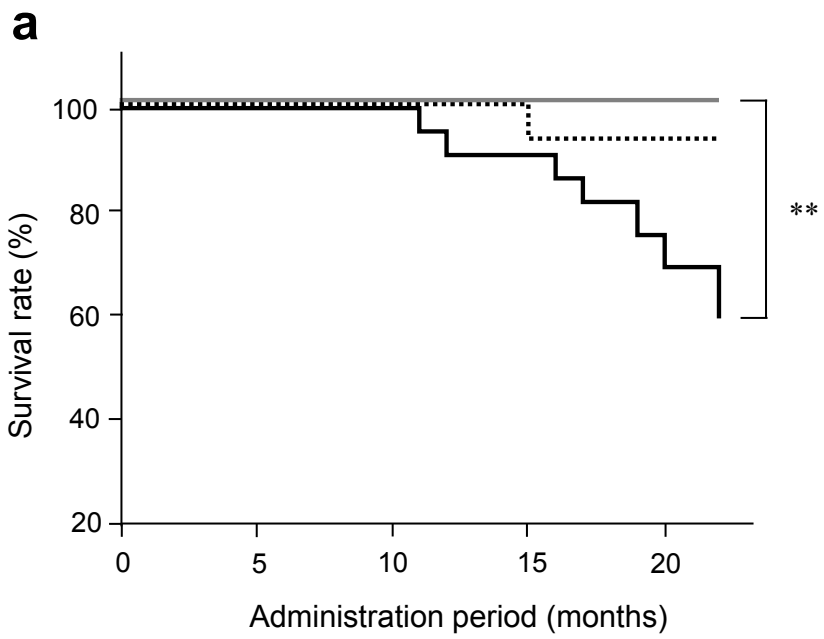
a
100
80
60
40
20
Survival rate (%)
0
5
10
15
20
Administration period (months)
**

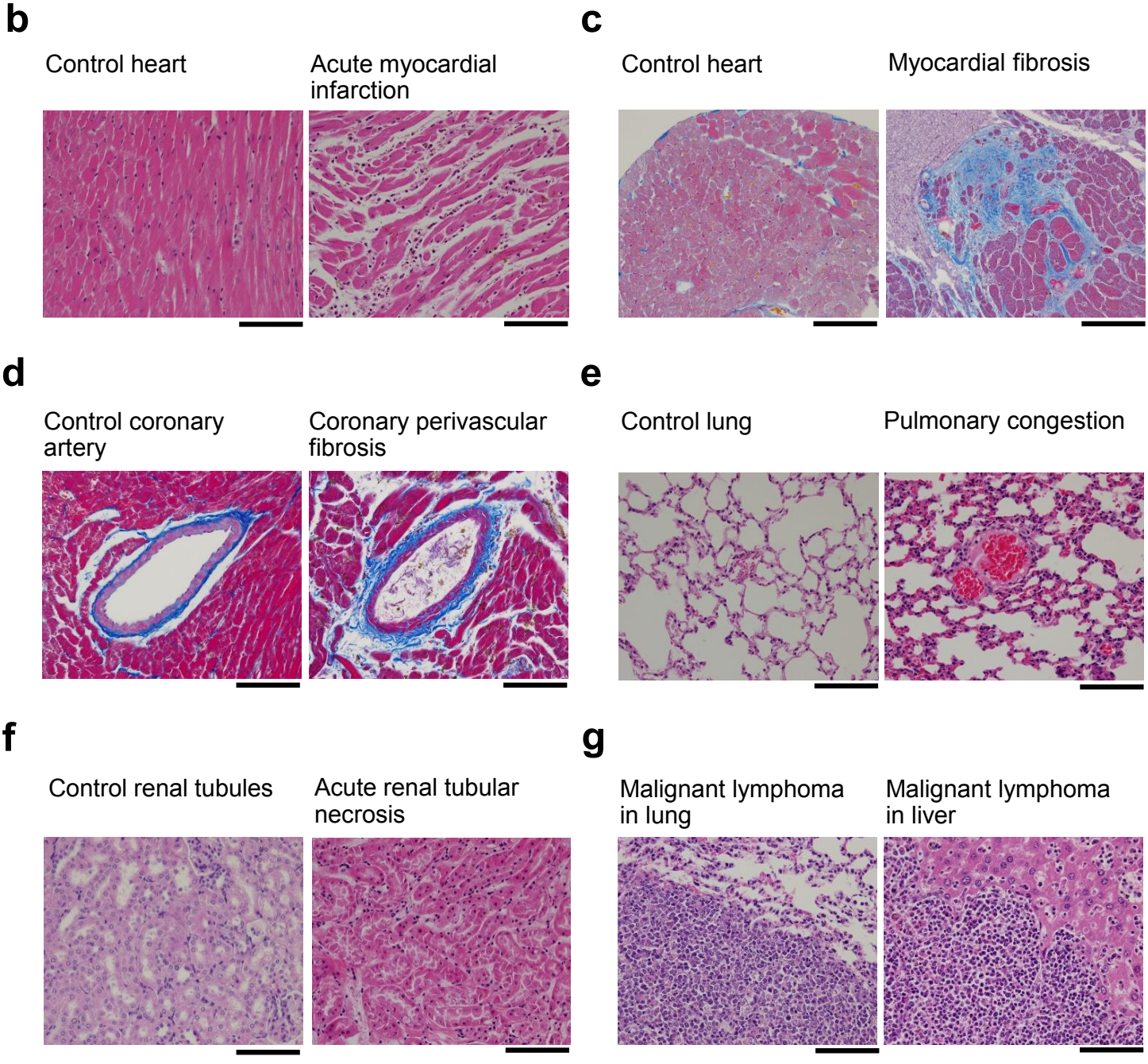
b
Control heart
Acute myocardial infarction
c
Control heart
Myocardial fibrosis
d
Control coronary artery
Coronary perivascular fibrosis
e
Control lung
Pulmonary congestion
f
Control renal tubules
Acute renal tubular necrosis
g
Malignant lymphoma in lung
Malignant lymphoma in liver

Fig. 8

Electronic Supplementary Material (ESM) Methods

Mice

This study was reviewed and approved by the Animal Care and Use Committee, the University of the Ryukyus, Japan, and was carried out according to the Institutional Policy on the Care and Use of the Laboratory Animals. The experiments were performed in 6-week-old male wild-type C57BL/6J mice (Kyudo, Co., Inc., Tosu, Japan). All the mice were maintained in temperature- and humidity-controlled rooms illuminated from 8:00 a.m. to 8:00 p.m. Food and water intake was measured by placing the animals in metabolic cages (Metabolica, type MM-ST, Sugiyama-Gen Iriki, Co., Inc., Tokyo, Japan) for 24 hours.

Diet

We prepared a purified amino acid-based low nitrite and nitrate chow in which the contents of L-arginine (14.1 g/kg), fat (13.5% of total energy), carbohydrates (58.0% of total energy), protein (28.5% of total energy), and energy (17.2 kJ/g) were identical to a regular chow (Purina 5001, LabDiet, St. Louis, MO). The composition of the amino acid-based low nitrite/nitrate chow was as follows (g/kg): L-alanine 17.0, L-arginine HCl 14.1, L-aspartic acid 33.3, L-cystine 3.7, L-glutamic acid 51.96, glycine 14.4, L-histidine HCl monohydrate 6.8, L-isoleucine 13.5, L-leucine 21.7, L-lysine HCl 16.7, L-methionine 7.9, L-phenylalanine 12.3, L-proline 17.7, L-serine 14.1, L-threonine 10.8, L-tryptophan 3.4, L-tyrosine 8.4, L-valine 14.0, sucrose 270.3, corn starch 150.0, maltodextrin 150.0, soybean oil 59.22, cellulose 30.0, mineral mix (AIN-93M-MX) 35.0, calcium phosphate 8.2, vitamin mix (AIN-93-VX) 13.0, choline bitartrate 2.5, and tertiary butylhydroquinone 0.02 (Oriental Yeast Co., Ltd., Tokyo, Japan). Nitrite and nitrate levels were not detected in the low nitrite/nitrate chow. We also prepared potable ultrapure milli Q water in which nitrite and nitrate levels were undetectable

(Merck Millipore, Darmstadt, Germany). Either the low nitrite/nitrate chow plus ultrapure water (low nitrite/nitrate diet, LND) or the regular chow plus tap water (regular diet, RD) was fed *ad libitum* to the mice from 6 weeks of age for 1.5-22 months. In some experiments, 2 mmol/l sodium nitrate (Wako Pure Chemical Industries, Ltd., Osaka, Japan) in the ultrapure water were administered in the mice fed the low nitrite/nitrate diet from 6 weeks of age for 1.5-22 months. The water was made fresh three times a week.

Nitrite and Nitrate Levels

The nitrite and nitrate contents in the chows were analysed by the diazotization method and the cadmium reduction-diazotization method, respectively (Japan Food Research Laboratories, Tokyo, Japan), and the detection limit of nitrite and nitrate was 6.5 and 4.8 μmol/kg, respectively. The nitrite and nitrate levels in the plasma and drinking water were assessed by the HPLC-Griess system using an Eicom NOx analyser (ENO-20, Eicom, Kyoto, Japan), and the detection limit of nitrite and nitrate was 0.01 and 0.01 μmol/l, respectively.

Blood Pressure

Systolic blood pressure was measured by the tail-cuff method under conscious conditions in a blind manner (Model MK-2000, Muromachi Kikai, Co., Inc., Tokyo, Japan). They were measured at the same time of day (9:00-11:00 a.m.) in consideration of the circadian rhythm of blood pressure levels.

Glucose Tolerance Test

A glucose tolerance test was performed under general anaesthesia with sodium pentobarbital (50 mg/kg, IP, Sigma-Aldrich, St. Louis, MO, USA) after 18 hours of fasting. One g of glucose per kg body weight was intraperitoneally injected into the

mice. Whole blood samples were collected from the tail at indicated time points, and the blood glucose levels were evaluated by a portable blood glucose analyser (Glucocard MyDia, Arkray, Inc., Kyoto, Japan).

Insulin Tolerance Test and Plasma Insulin

An insulin tolerance test was carried out under general anaesthesia with sodium pentobarbital (50 mg/kg, IP). The mice received 0.3 unit/kg body weight insulin (Eli Lilly, Indianapolis, IN) injected into the intraperitoneal cavity. Data are expressed as percent change of blood glucose levels to a basal blood glucose level at time 0. The fasting plasma insulin levels were assessed by a commercially available ELISA kit (AKRIN-031, Shibayagi, Gunma, Japan).

Visceral Fat Weight

After euthanasia, epididymal white adipose tissues (EWAT) were removed and weighed. Data are expressed as the ratio of EWAT weight to body weight.

Adipocyte Hypertrophy and Inflammation

Epididymal and peri-renal white adipose tissues (WAT) were weighted and immersed in a 4% paraformaldehyde solution. Whole tissues were embedded in paraffin to obtain maximal cut surface, and 10-μm-thick serial slices were stained with a haematoxylin-eosin solution. The sections were scanned with a light microscope equipped with a 2-dimensional analysis system (IBAS, Carl Zeiss, Jena, Germany). The circumferential length of each adipocyte was measured by a light microscope equipped with a CCD camera and morphometric analysis software (DS-Ri1CCD camera and NIS-Elements D 3.2 software, Nikon, Tokyo, Japan). We assumed that each adipocyte was circular in shape, and calculated the adipocyte cross-sectional area from the formulas of the length ($2\pi r$) and area (πr^2). One hundred

adipocytes were evaluated in each animal, and the mean value was used for statistical analysis. In visceral adipose tissues of mice fed the LND, aggregates of inflammatory cells that were composed of lymphocytes, histiocytes, or a few plasma cells were observed. For evaluation of inflammation in the adipose tissues, aggregates of inflammatory cells (inflammatory foci consisting of more than 10 inflammatory cells) were counted in the maximal cut surface of the epididymal and the peri-renal WAT sections on a light microscope at 40x magnification. The degree of inflammation was evaluated by the number of inflammatory foci.

Plasma Lipid Profile

Blood was collected by cardiac puncture after 18 hours of fasting under general anaesthesia with sodium pentobarbital (50 mg/kg, IP). The blood samples were centrifuged at 3,000 rpm, 4˚C, for 15 min, and the supernatants were stored at –80˚C. Plasma lipid profile was assessed by a Dri-Chem autoanalyser (FDC4000, Fuji Film Co., Ltd., Tokyo, Japan). Plasma low-density lipoprotein (LDL) cholesterol levels were determined by the high-sensitivity lipoprotein profiling system using high-performance liquid chromatography (Skylight Biotech Inc., Akita, Japan) [1].

Western Blot Analysis

Western blot analysis was performed as we previously reported [2]. Immediately after euthanasia, the aortas and adipose tissues were quickly excised under general anaesthesia with sodium pentobarbital (50 mg/kg, IP) and frozen in liquid nitrogen. The tissues were homogenized in 0.5 ml of ice-cold homogenization buffer containing 50 mmol/l Tris (pH 8.0), 150 mmol/l NaCl, 0.1% SDS, 20 mmol/l 3-[(3-cholamidepropyl) dimethylammonio]-1-propanesulphonate, and 0.5% protease inhibitor cocktail (Roche, Mannheim, Germany). The tissue homogenates were

centrifuged at 15,000 *g* for 10 min at 4°C, and the supernatants were used for Western blot analysis. To detect neuronal (nNOS), inducible (iNOS), and endothelial NO synthase (eNOS), phosphorylated eNOS at serine 1177 and at threonine 495 (BD Transduction Laboratories, Franklin Lakes, NJ), adiponectin, peroxisome proliferator-activated receptor-γ (PPAR-γ), adenosine monophosphate-activated protein kinase (AMPK), sirtuin1 (Cell Signaling Technology, Danvers, MA), phosphorylated AMPK (p-AMPK, Santa Cruz Biotechnology Inc., Dallas, TX) and glyceraldehyde-3-phosphate dehydrogenase (GAPDH) (Sigma-Aldrich), 20-50 μg protein were solubilized in a Laemmli sample buffer containing 2.5% 2-mercaptoethanol at 80°C for 5 min, and subjected to 6-10% SDS-PAGE at room temperature. The gels were transferred to PVDF membranes, and the membranes were blocked with 5% nonfat milk. They were then incubated with antibodies for NOS (1:1000), adiponectin (1:1000), PPAR-γ (1:500), AMPK (1:500), sirtuin1 (1:500), p-AMPK (1:500), or GAPDH (1:10000) in 5% non-fat milk and Tris-buffered saline-Tween. After being washed and incubated with a horseradish peroxidase-conjugated anti-mouse IgG antibody (1:1000) or an anti-rabbit IgG antibody (1:1000), the membranes were developed with an enhanced chemiluminescence system (Western Lightning ECL Pro, PerkinElmer Inc., Waltham, MA). Quantitative densitometry was performed by a lumino-image analyser (LAS-4000 mini EPUV, Fuji Film) and Multi Gauge software (version 3.0).

16S Ribosomal RNA Gene Sequencing

Immediately after euthanasia, the faecal contents of the ceca were aseptically collected by manual extrusion, and quickly frozen and stored at -80°C. These procedures were performed at the same time of day (10:00-12:00 a.m.) in consideration of the circadian rhythm of the gut microbiome. Faecal DNA was isolated by using a QIAamp Fast DNA stool Mini kit (QIAGEN, Hilden, Germany). The faecal DNA samples were

subjected to a next generation sequencer, as reported previously [3]. The number of each bacterial strain contained in the faecal contents was estimated as the genome equivalent by quantitative real-time PCR of 16S ribosomal RNA genes, followed by pyrosequencing of the 16S amplicons, as reported previously [3].

Organ Chamber Experiment

The thoracic aortas were excised and placed in a cold Krebs-Henseleit solution (KHS). Fat and connective tissues were removed from the thoracic aortas, and 1.5 mm-long aortic ring segments were made. The composition of the KHS (pH 7.4) was (mmol/l): NaCl 120, KCl 4.8, $CaCl_2$ 1.25, $MgSO_4$ 1.2, KH_2PO_4 1.2, $NaHCO_3$ 25.0 and glucose 11.0. The ring preparations were mounted on stainless steel hooks under a resting tension of 0.1 g in a microtissue organ bath (MTOB-1, Labo Support, Osaka, Japan) containing KHS aerated with 95% O_2 and 5% CO_2 at 37°C. The isometric contractile force of the ring preparations was recorded. After 60 min of stabilization, the ring preparations were contracted with KCl (45 mmol/l) in order to test their viability, and thereafter rinsed three times with KHS. Contractile responses of the ring preparations to phenylephrine (10^{-9} to 10^{-5} mol/l) and vasorelaxant responses of phenylephrine (10^{-6} mol/l)-precontracted rings to acetylcholine (10^{-9} to 10^{-5} mol/l) or diethylamine NONOate (10^{-9} to 10^{-5} mol/l) were evaluated. These vasoactive agents were cumulatively added to the organ bath. At the end of the experiments, each segment was maximally relaxed by adding 10^{-4} mol/l papaverine hydrochloride.

Micro-Computed Tomography (CT) Imaging

Mice were anesthetized with 2% isoflurane (Wako Pure Chemical), and CT images were acquired by three-dimensional micro-CT (R_mCT2; Rigaku Corporation, Tokyo, Japan) with a resolution of 148×148×148 μm^3, a tube voltage of 90 kV, and a tube current of 160 μA. The exposure time was 34 seconds, and tomographic images were obtained

retrospectively at the expiration breathing phase. The CT images were visualized and analysed by CTAtlas Metabolic Analysis Ver. 2.03 software (Rigaku Corporation). The body fat was measured from the base of the ensiform cartilage to the pelvic floor and analysed to divide into visceral and subcutaneous fat.

Statistical Analyses

Most results are expressed as mean ± SEM. Statistical analyses were performed by a two-sided Student's *t*-test, or one-way or two-way ANOVA followed by Bonferroni's *post hoc* test for multiple comparisons. Results of sequencing reads of gut bacteria in the hierarchy of ranks are indicated as median and interquartile range, and the statistical analysis was carried out by a Wilcoxon rank-sum test, as previously reported [4]. Kaplan-Meier survival curves were plotted by GraphPad Prism 6.0 software (Graphpad Software, San Diego, CA) and were compared by the log-rank test. A value of $P<0.05$ was considered to be statistically significant.

References

[1] Usui S, Hara Y, Hosaki S, Okazaki M (2002) A new on-line dual enzymatic method for simultaneous quantification of cholesterol and triglycerides in lipoproteins by HPLC. J Lipid Res 43: 805-814

[2] Uchida T, Furuno Y, Tanimoto A, et al. (2014) Development of an experimentally useful model of acute myocardial infarction: 2/3 nephrectomized triple nitric oxide synthases-deficient mouse. J Mol Cell Cardiol 77: 29-41

[3] Kim SW, Suda W, Kim S, et al. (2013) Robustness of gut microbiota of healthy adults in response to probiotic intervention revealed by high-throughput pyrosequencing. DNA Res 20: 241-253

[4] Qin N, Yang F, Li A, et al. (2014) Alterations of the human gut microbiome in liver cirrhosis. Nature 513: 59-64

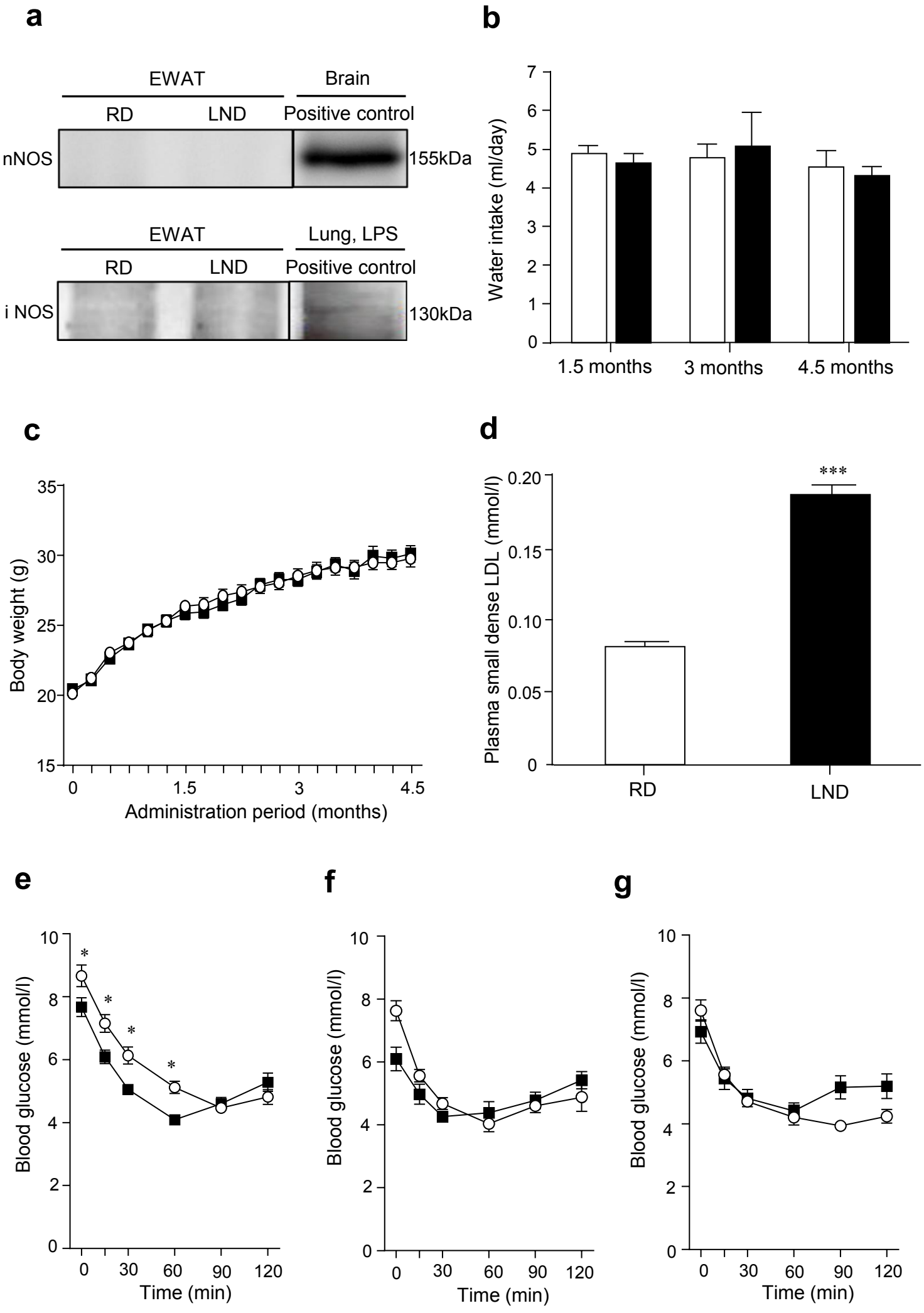
a
EWAT
Brain
RD
LND
Positive control
nNOS
155kDa
EWAT
Lung, LPS
RD
LND
Positive control
i NOS
130kDa
b
Water intake (ml/day)
1.5 months
3 months
4.5 months
c
Body weight (g)
Administration period (months)
d
Plasma small dense LDL (mmol/l)
***
RD
LND
e
Blood glucose (mmol/l)
Time (min)
f
Blood glucose (mmol/l)
Time (min)
g
Blood glucose (mmol/l)
Time (min)

ESM Fig. 1

ESM Fig. 1

Effects of 1.5-4.5 months of LND on NOS expression, water intake, body weight, small dense LDL, and blood glucose in WT mice. **a**, Representative Western blots of nNOS and iNOS in the EWAT after 3 months of LND. **b**, Water intake (n=10-12). White bars; RD, black bars; LND. **c**, Body weight (n=12). White circles; RD, black squares; LND. **d**, Plasma small dense LDL cholesterol levels induced by 3 months of LND (n=12). **e-g,** Blood glucose levels after intraperitoneal injection of 0.3 unit/kg insulin after 1.5 (**e**), 3 (**f**), and 4.5 (**g**) months of LND (n=8-12). White circles; RD, black squares; LND. *$p<0.05$ and ***$p<0.001$.

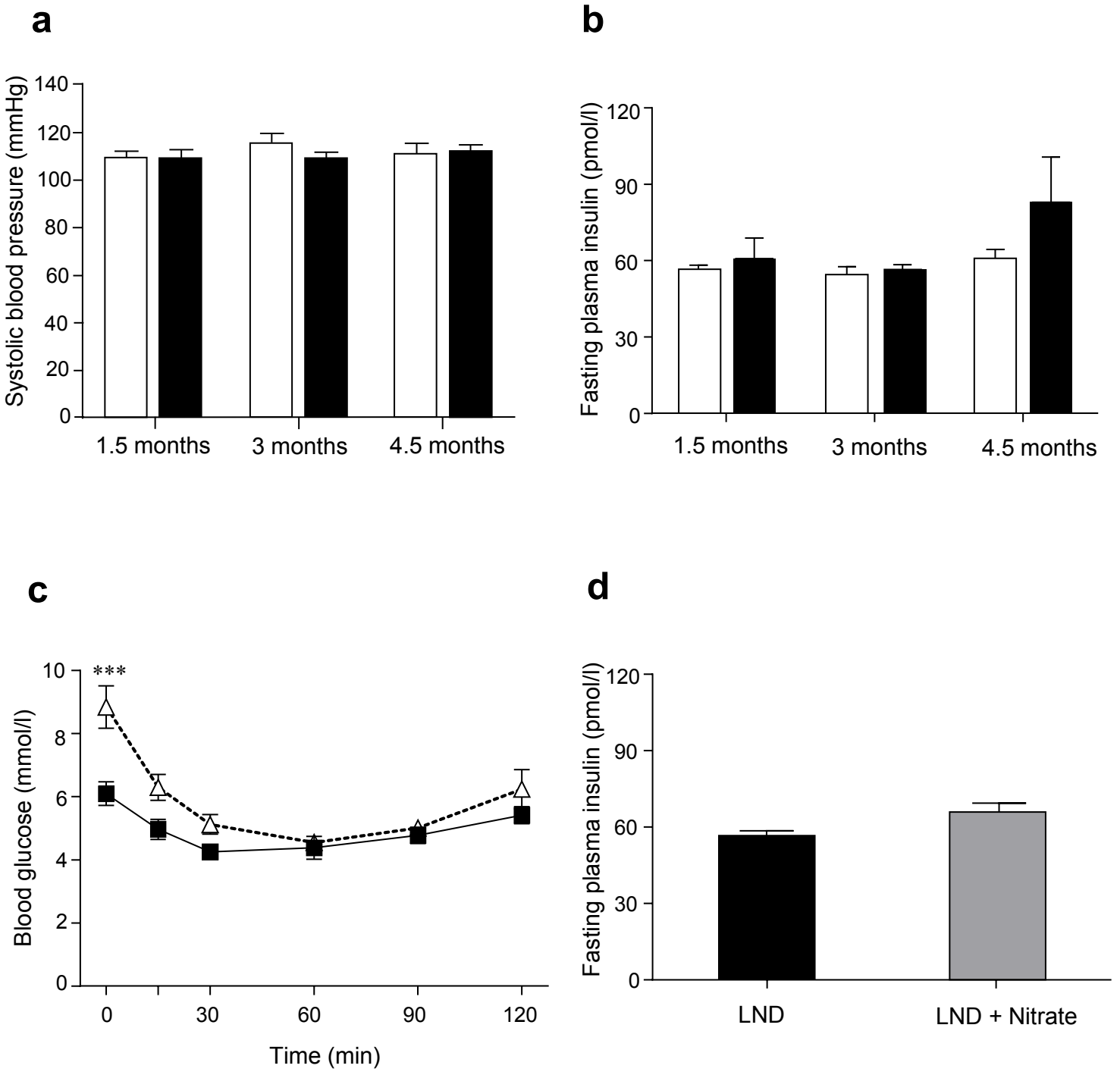

ESM Fig. 2
Effects of 1.5-4.5 months of LND or nitrate supplementation on blood pressure, plasma insulin, and blood glucose. **a**, Systolic blood pressure (n=12). White bars; RD, black bars; LND. **b**, Fasting plasma insulin levels (n=10-12). White bars; RD, black bars; LND. **c,** Blood glucose levels after intraperitoneal injection of 0.3 unit/kg insulin following 3 months of LND or nitrate supplementation (n=9-10). Black squares; LND, white triangles; LND + Nitrate. **d**, Fasting plasma insulin levels after 3 months of LND or nitrate supplementation (n=10-12). ***p<0.001.

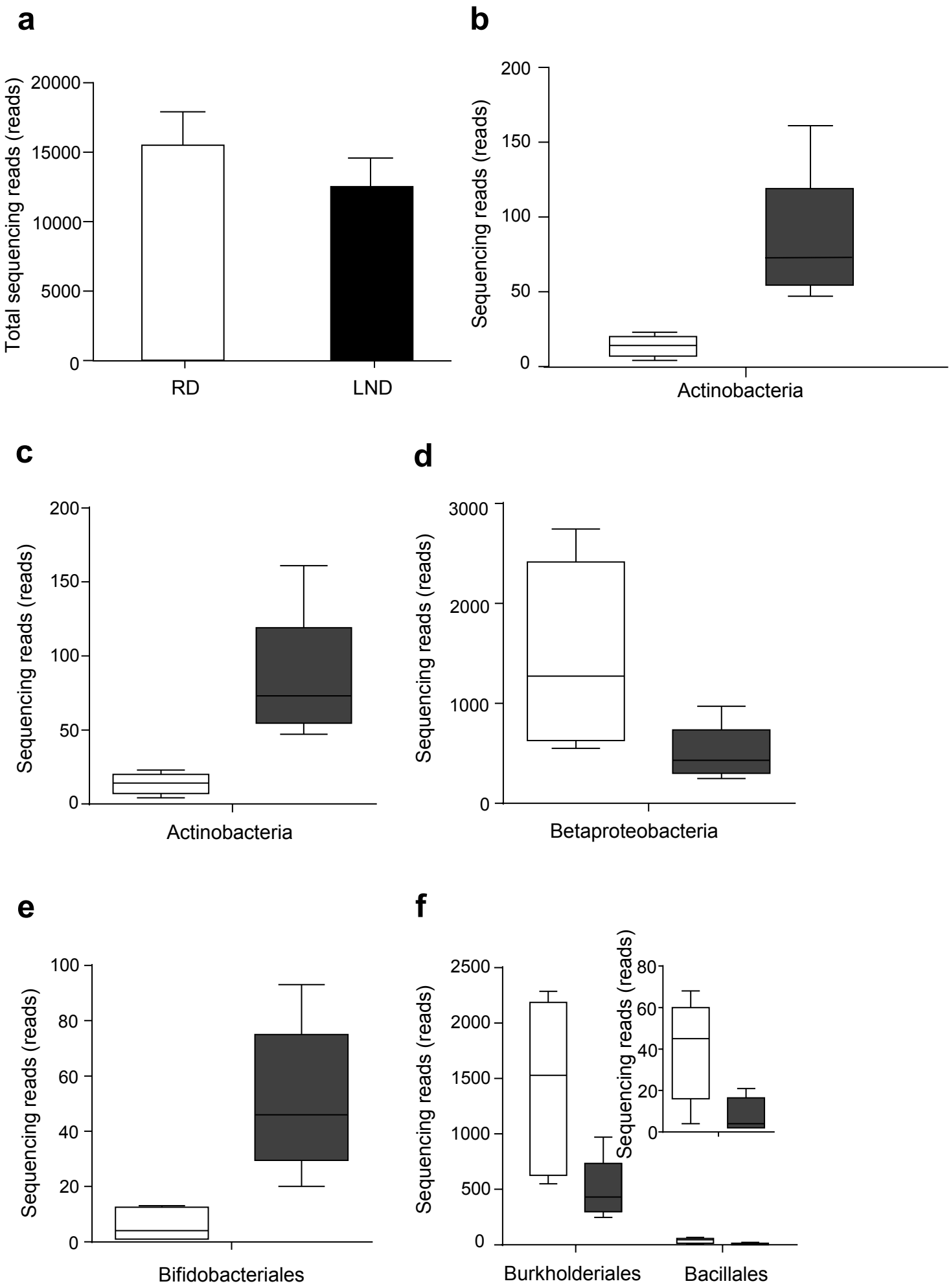
a
Total sequencing reads (reads)
20000
15000
10000
5000
0
RD
LND
b
Sequencing reads (reads)
200
150
100
50
0
Actinobacteria
c
Sequencing reads (reads)
200
150
100
50
0
Actinobacteria
d
Sequencing reads (reads)
3000
2000
1000
0
Betaproteobacteria
e
Sequencing reads (reads)
100
80
60
40
20
0
Bifidobacteriales
f
Sequencing reads (reads)
2500
2000
1500
1000
500
0
Sequencing reads (reads)
80
60
40
20
0
Burkholderiales
Bacillales

ESM Fig. 3 a-f

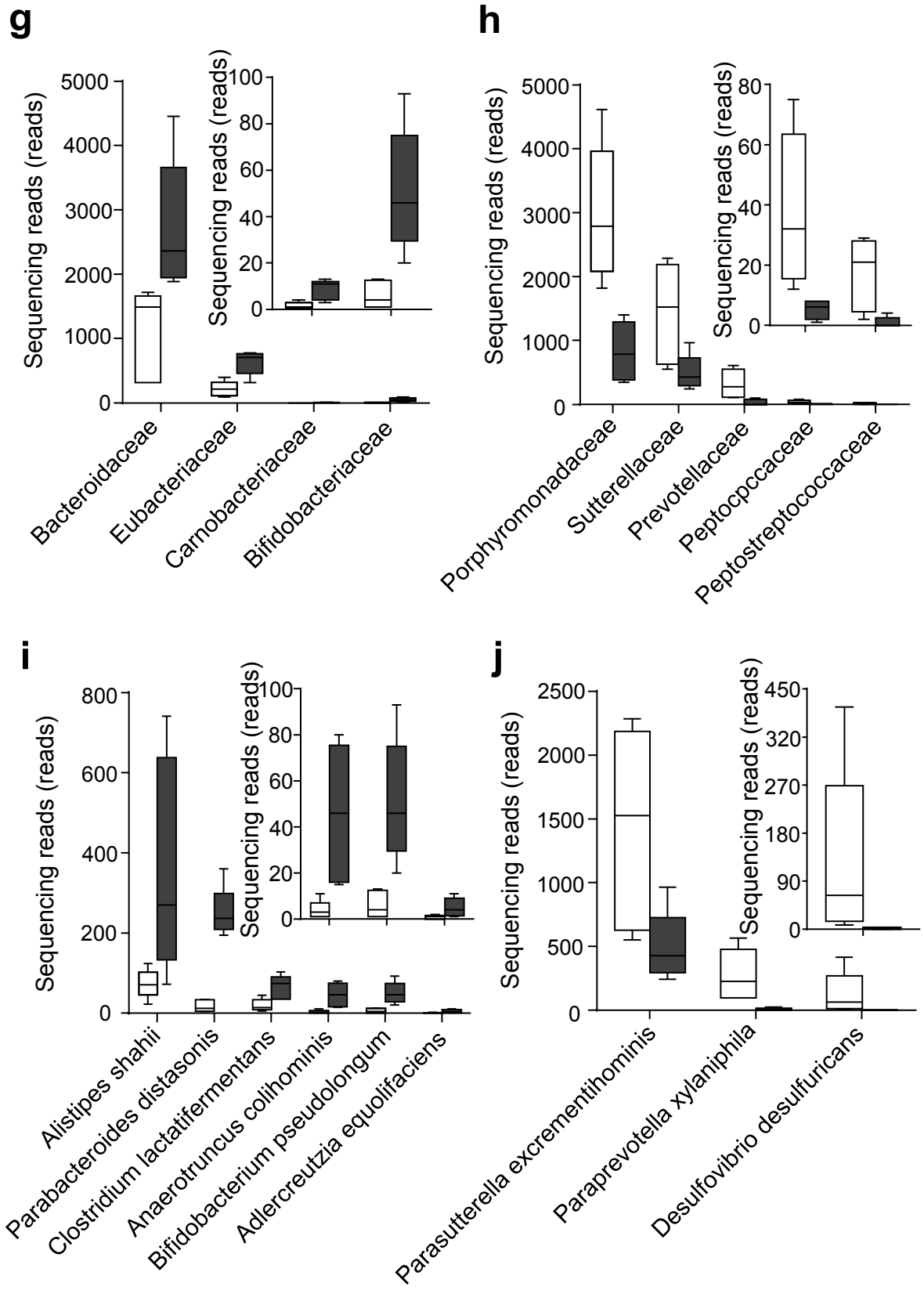

ESM Fig. 3

Effects of 3 months of LND on gut microbiota. **a**, Total sequencing reads (n=5 each). **b-j**, Significantly higher gut bacteria in phylum (**b**), class (**c**), order (**e**), family (**g**) and species (**i**) rank and significantly lower gut bacteria in class (**d**), order (**f**), family (**h**) and species (**j**) rank (p<0.05, n=5 each). Insets are the magnified views of sequencing reads of the rightmost gut bacteria. White boxes; RD, grey boxes; LND.

ESM Fig. 3 g-j

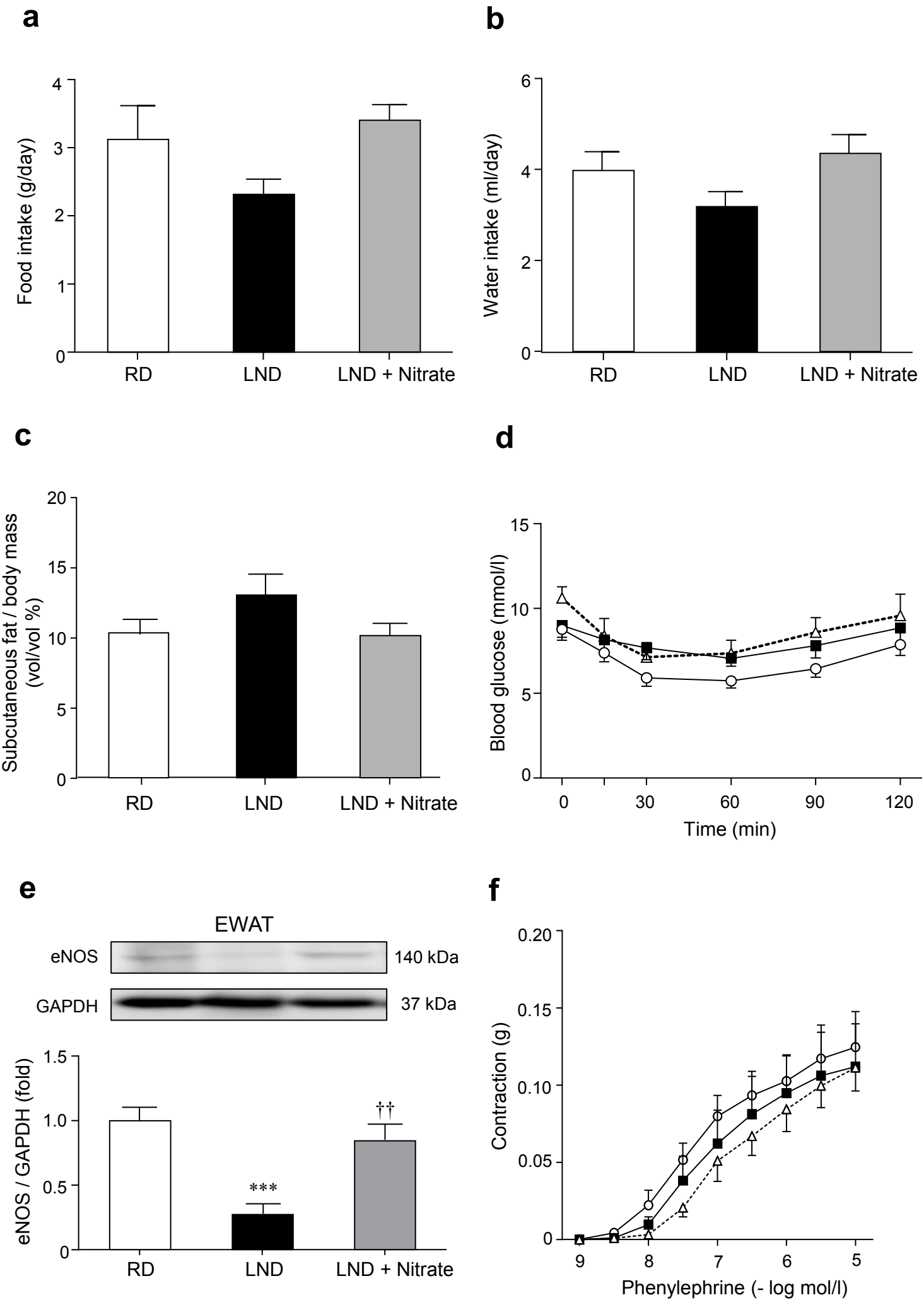
a
Food intake (g/day)
RD
LND
LND + Nitrate
b
Water intake (ml/day)
RD
LND
LND + Nitrate
c
Subcutaneous fat / body mass (vol/vol %)
RD
LND
LND + Nitrate
d
Blood glucose (mmol/l)
Time (min)
e
EWAT
eNOS
140 kDa
GAPDH
37 kDa
eNOS / GAPDH (fold)
***
††
RD
LND
LND + Nitrate
f
Contraction (g)
Phenylephrine (- log mol/l)

ESM Fig. 4 a-f

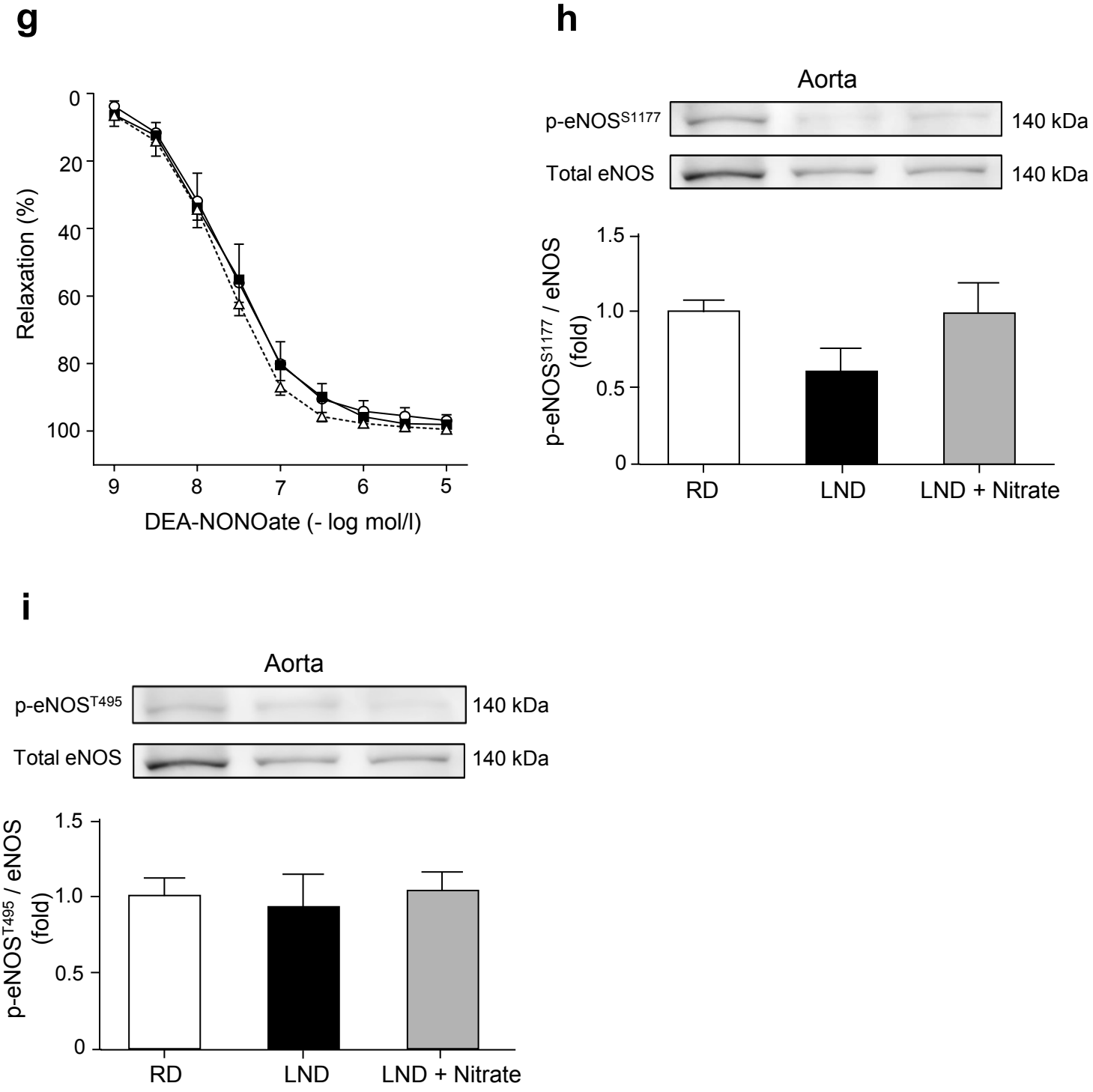

ESM Fig. 4

Effects of 18 months of LND and nitrate supplementation on food and water intake , subcutaneous fat, vascular reactivity, and eNOS. **a,b,** Food and water intake (n=12). **c**, Subcutaneous fat-to-body mass (n=11-12). **d,** Blood glucose levels after intraperitoneal injection of 0.3 unit/kg insulin (n=6-7). White circles; RD, black squares; LND, white triangles; LND + Nitrate. **e**, eNOS protein levels in the EWAT (n=6). **f**, Contractions to phenylephrine (n=6). White circles; RD, black squares; LND, white triangles; LND + Nitrate. **g**, Endothelium-independent relaxations to DEA-NONOate (n=6). White circles; RD, black squares; LND, white triangles; LND + Nitrate. **h**, eNOS phosphorylation levels at serine 1177 in the aorta (n=6). **i**, eNOS phosphorylation levels at threonine 495 in the aorta (n=6). ***p<0.001 in RD vs. LND; ††p<0.01 in LND vs. LND + Nitrate.